Lawrence Berkeley National Laboratory

Lawrence Berkeley National Laboratory

Title

LATTICE IMAGING AND MECHANICAL PROPERTIES OF A Cu-Ni-Cr SPINODAL ALLOY

Permalink

https://escholarship.org/uc/item/7vz0v0s6

Author

Wu, C.-K.

Publication Date

1976-12-01

eScholarship.org Powered by the California Digital Library
University of California

0 0 0 0 4 6 0 8 1 6 3

LBL-5729
c 1

LATTICE IMAGING AND MECHANICAL PROPERTIES OF A Cu-Ni-Cr SPINODAL ALLOY

Chien-Kuo Wu
(M. S. thesis)

RECEIVED
LAWRENCE
BERKELEY LABORATORY
FEB 15 1977
LIBRARY AND
DOCUMENTS SECTION

December 1976

Prepared for the U. S. Energy Research and
Development Administration under Contract W-7405-ENG-48

For Reference

Not to be taken from this room

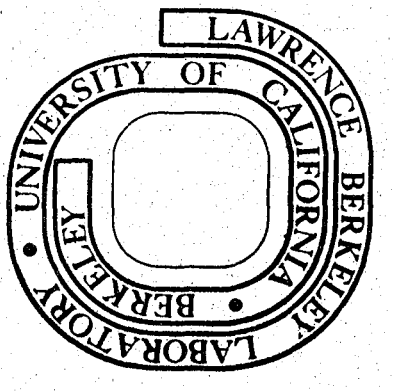

LBL-5729
c.1

LEGAL NOTICE

This report was prepared as an account of work sponsored by the United States Government. Neither the United States nor the United States Energy Research and Development Administration, nor any of their employees, nor any of their contractors, subcontractors, or their employees, makes any warranty, express or implied, or assumes any legal liability or responsibility for the accuracy, completeness or usefulness of any information, apparatus, product or process disclosed, or represents that its use would not infringe privately owned rights.

0 0 0 3 4 6 3 3 1 5 4

LATTICE IMAGING AND MECHANICAL PROPERTIES OF A Cu-Ni-Cr SPINODAL ALLOY

Chien-Kuo Wu

Table of Contents

0 0 - 0 4 6 3 1 6 5

LATTICE IMAGING AND MECHANICAL PROPERTIES OF A Cu-Ni-Cr SPINODAL ALLOY

Chien-Kuo Wu

ABSTRACT

A commercially important Cu-28.9%Ni-2.8%Cr alloy has been heat-treated to produce spinodal structures. Conventional transmission electron microscopy (TEM) and diffraction have been used to study the spinodally decomposed product and to measure the wavelengths in the specimens. Tensile tests were performed to measure mechanical properties of the aged samples, and the fracture surfaces were examined by scanning electron microscopy.

The lattice imaging technique of high-resolution electron microscopy has been applied to study the compositional fluctuations in this alloy. Although the change of lattice parameter between the two phases is only $\sim$1%, characteristic spinodal composition waves can be detected by lattice imaging, both in the early and later stages of aging. The reliability of various methods for processing the imaging data are discussed. The correlation of mechanical properties with microstructure then shows a dependence of yield stress increment on lattice parameter change between the two phases.

0 0 3 4 6 0 3 1 5 5

I. INTRODUCTION

The object of this research is to investigate experimentally the spinodal characteristics of an alloy and then correlate the mechanical properties with the changes in microstructure during spinodal decomposition and particle coarsening. Cu-Ni-Cr was chosen particularly for its commercial importance as an alloy of excellent strength and corrosion resistance in marine environments.[1] Conventional thermal heat treatments were performed and mechanical property data were obtained by standard methods and the microstructure was studied by transmission electron microscopy. A relative recent development viz. lattice imaging was also employed to obtain information concerning the alloy at the atomic level.

A. Spinodal Decomposition

Spinodal decomposition is a mechanism of homogeneous phase transformation which usually produces a uniform microstructure. It was first described for chemical solutions by J. Willard Gibbs[2] in the 1880's. Thermodynamically, the spinodal can be described as the condition that the second derivative of the free energy with respect to composition is zero ($\frac{\partial^2 F}{\partial C^2} = 0$). Inside the spinodal, where $\frac{\partial^2 F}{\partial C^2} < 0$, the unstable solid solution decomposes spontaneously into two phases, because there is no activation barrier for nucleation. Therefore Gibbs referred to the spinodal as the limit of metastability.

It is only very recently that extensions of spinodal phenomena to metallurgical theory and solid solution reactions have been described

fully. Hillert[3] and Cahn[4,5] contributed to the development of theories of spinodal decomposition. They used a diffusion theory, based on changes in the solution free energy with composition fluctuations in the unstable solid solution.

In solids, there are two aspects of the spinodal that require special mention. Firstly, the spinodal implies that the new phase forms by a continuous process. Thus the kinds of solid phases formed are crystallographically quite similar to the original phase. The simplest cases are those when the two phases have the same crystal structures and differ only in composition. Secondly, this continuous process means initially that the two phases are coherent with each other and the lattice remains continuous.

Spinodal decomposition can also be described by small composition fluctuations over large distances, while a classical nucleation process is described by large composition variations over small distances.

The microstructures of a spinodally decomposed alloy can be characterized by these parameters:

(1) Volume fraction of the two phases;

(2) Wavelength of the modulations;

(3) Amplitude of the composition fluctuations.

Analyses of these parameters in spinodal Cu-Ni-Fe alloys have been performed by Butler and Thomas,[6] and Livak and Thomas.[7] Their experimental results revealed that, while coherency is maintained, the yield stress is directly proportional to the difference in cubic lattice parameters of the two precipitating phases, and is independent of the wavelength and volume fractions in symmetric and assymmetric Cu-Ni-Fe

0 0 - 0 4 6 3 3 1 6 7

alloys. However, very few systematic studies of other systems have been performed to investigate the relationship of mechanical properties with the microstructural parameters of spinodal alloys. Therefore, it is the purpose of this research to explore these parameters and to establish these relationships in a commercial Cu-Ni-Cr alloy.

B. The Material

The constitutional studies by Meijering et al.[8] (Fig. 1) have shown that for Cu-Ni-Cr, the alloy studied in the present research, there is a miscibility gap in the face-centered cubic phase diagram of the system, although binary Cu-Ni alloys are completely miscible. Badia, Kirby and Mihalisin[9] have studied the strengthening during continuous cooling of Cu-Ni-Cr alloys containing 20 to 45% Ni with up to 4% Cr. Their experimental observations showed many points of similarity with the theoretical calculations of Huston, Cahn and Hilliard[10] for spinodal decomposition during continuous cooling.

Spinodal decomposition during continuous cooling is of technological interest since continuous cooling will afford a convenient method of producing spinodal structures in commercial heat treating practice. From the literature,[1] the present Cu-Ni-Cr alloy undergoes spinodal decomposition when aging at temperatures below 760°C. This decomposition results in producing a microstructure of Cu-rich and Ni-Cr rich regions which both have face-centered cubic structures, and the lattice parameters of the two regions after heat-treating at 750°C are 3.603Å and 3.571Å,[8,9] respectively.

In this research, the alloys were aged at two temperatures (600°C and 700°C) to produce the spinodal structure, and the changes in microstructure and wavelength with aging time were followed by transmission electron microscopy and diffraction. The resulting periodic structure gives rise to the side-bands in diffraction patterns, typical of periodic spinodal systems. Also, the mechanical behavior of the spinodally decomposed and aged alloys was experimentally studied.

In order to correlate the mechanical properties with microstructure, the difference in lattice parameters of the two phases has to be determined.[11] Since the present material is non-magnetic, there is no Curie-temperature and so this method[6] cannot be applied to estimate the amplitudes of the composition fluctuations. Hence, for the purpose of obtaining an accurate measurement of Δa down to the atomic level, lattice imaging has been utilized to meet this requirement.

C. Lattice Imaging

The most common modes of operation of the transmission electron microscope are the formation of an image using only the transmitted electron beam (bright-field image) or one diffracted beam[12] (dark-field image). If an aperture is placed at the back focal plane of the objective lens to encircle both the transmitted spot and one diffracted spot, then the interference between these two spots will, under appropriate circumstances, give a set of fringes corresponding to the lattice planes in the crystal which give rise to the diffracted spot. This is a very useful method called lattice imaging which is capable of resolving the

0 0 0 4 6 0 0 1 6 8

microstructures of materials down almost to the atomic level. In order to achieve this, electron microscopes must have adequate resolution [13] (low spherical aberration constants for the objective lens).

Since spinodal decomposition is characterized as small composition fluctuations over a large distance, previous studies by X-ray diffraction and conventional transmission electron microscopy revealed only the wavelengths of the early stage composition modulations through diffracted intensities averaged over a large specimen area. The conventional bright-field or dark-field images of TEM cannot provide any compositional information about the two phases. It is only possible to detect the localized, plane-by-plane variations in composition by corresponding lattice parameter modulations through the lattice imaging technique.[13-16]

Recently, high-resolution lattice imaging of TEM has proved to be one of the most powerful methods to obtain information down to the atomic level in alloys. By directly imaging the lattice, finer detail can be observed concerning defects and phase transformation processes.

For instance, Sinclair, Schneider, and Thomas[14] analyzed ordering in Cu_3Au by this method. Their results have cleared up some problems and have given new structural information in a well-known system and illustrate the power of the technique for showing detail at the atomic level.

Gronsky, Okada, Sinclair, and Thomas[15] used the same method for spinodal alloys. In their preliminary results of spinodally decomposed Au-77 at. % Ni ($\Delta a \sim 14\%$) alloy, they were able to detect lattice parameter differences of up to 11% from one region to another by measurements on microdensitometer traces across the lattice fringes.[16] The average

wavelength determined from this technique is $\lambda \sim 29\text{Å}$ which is in agreement with that ($\lambda \sim 29\text{Å}$) determined from the positions of satellite reflections in the corresponding diffraction patterns. The lattice image of this material shows the principal features expected of a spinodally decomposed alloy.

A new approach using lazer optical diffraction[16] from the lattice imaging negatives allows areas as small as 10Å in diameter to be used to give diffraction data which is a considerable advance in terms of resolution over conventional diffraction methods. This helps in the interpretation of the lattice fringe images.

For the present research, since the difference in lattice parameters of the two phases is quite small ($(\Delta a)_{max} \sim 0.04\text{Å}$), the analysis of the lattice fringes in this way must be done very carefully. In order to obtain meaningful results from the lattice images, three different methods were used to determine Δa which then proved to be consistent with one another.

In Cu-Ni-Cr alloy, spinodal decomposition occurs along the cube directions, the so-called elastically "soft" directions. Therefore, (200) lattice fringes were imaged to measure Δa.

0 0 0 0 4 6 0 3 1 6 9

II. EXPERIMENTAL PROCEDURES

(1) The Sample

The sample is a commercial Cu-based alloy. Chemical analysis from Paul Merica Laboratory gives the following result, expressed in weight %:

Cu - balance	C - 0.014%
Ni - 28.9%	Ti - 0.051%
Cr - 2.84%	Si - 0.091%
Mn - 0.55%	Fe - 0.32%
Zr - 0.22%	

(2) Heat Treatment

The alloy was encapsulated in evacuated quartz tube, homogenized at 1100°C for 72 hours, quenched into ice brine and cold rolled down to 10 mils thickness for transmission electron microscope specimens.

After cutting and machining, the various experimental specimens were annealed in quartz tubes filled with purified argon at 1100°C for two hours and quenched again in ice brine.

Specimens were subsequently aged at 700°C and 600°C for various times from 5 min. to 808 hours.

(3) Tensile Test

For tensile test specimens, the alloy was first cut into strips (2" x 3" x 80 mils) and the heat-treatment subsequently performed. The strips were then machined into standard flat tensile specimens (Fig. 2).

The specimens were tensile pulled in an Instron machine. In order to investigate the fracture surface of the specimens, the specimens were examined in a scanning electron microscope operating at 20 kV.

(4) Polishing Procedures

The heat-treated alloys were chemically polished in a solution of 3 parts of HNO_3 and 1 part of HF at room temperature to a thickness of 3-5 mils, and mechanically polished on (600) grit emery paper. Small discs were punched from the alloys and thin foils for TEM were prepared by jet-electro polishing, with the following solutions and conditions:

solution: 125 ml nitric acid and 375 ml methanol

condition: temperature: -20°C to -25°C (cold methanol was used as a cooling bath)

polishing voltage: 20 V (DC)

Specimens were then observed in a Siemens IA Elmiskop for conventional electron microscopy.

(5) Lattice Imaging

For the lattice imaging technique, a Philips EM 301 transmission electron microscope equipped with high-resolution stage was utilized. The specimen grains with [001] parallel to the microscope optical axis were found and the crystal was then tilted such that two beam conditions with a strongly diffracted (200) spot was obtained in order to image (200) lattice fringes. These reveal the characteristics of spinodal decomposition along this direction.

0 0 4 0 4 6 0 8 1 7 0

(6) Calibration of the Magnification

Usually lattice imaging pictures were taken in the electron microscope operating at high magnification (over 5×10^5 times). The calibration of the exact magnification of the microscope is very important for any quantitative measurement on the lattice fringe spacings. Since the true magnification is only within ±10% limits of that normally shown on the microscope meter, the exact magnification was determined by the following procedures.

Firstly, the average lattice constant of the alloy at each aging condition was determined by standard X-ray diffraction methods. The average corresponding (200) lattice fringe spacings was established on enlarged micrographs and the calibration found for this particular picture.

(7) Measurement of Lattice Constants

Three different methods were used to measure the variations of lattice parameters between the two phases from lattice imaging negatives:

(a) Optical diffraction: The lattice imaging negatives were placed in the path of a HeNe lazer beam in a standard optical bench. The fringes present in the negatives give rise to diffraction spots in the back focal plane of the optical objective lens. Then by measuring the distance r between the transmitted and diffracted spots, using the formula:

$$\lambda L = rd$$

where λL is a constant, and by comparison with that of standard gold (200) fringes, then d, the corresponding lattice spacing giving rise to the diffracted spots, can be determined.

(b) Microdensitometer trace analysis: The individual lattice constants can be found by directly measuring the distance from peak to peak on a microdensitometer plot of the image and dividing by the appropriate magnification.

Here in this research, average values were obtained over 15 fringes at a time, and standard deviations were calculated to give the accuracy limits. The final shape of the curve will then show the variations of the lattice parameters.

(c) Direct measurement from enlarged micrograph. It is straightforward just to measure the lattice spacings on an enlarged micrograph, divide by the magnification and the lattice constants can be obtained immediately.

(8) Accuracy of Measurement

The three different methods used to measure the fringe spacings have been described above. Since the maximum difference of lattice parameters is so small ($\sim$1%), then the measurements must be done very carefully, and the accuracy of each method will be estimated as follows:

(a) Optical diffraction provides the most reliable results among the three methods. It converts fringe image information of lattice planes in the specimen into diffraction spots. By placing a certain size of aperture in the beam path, diffraction information can be obtained even from a very small area in the material.

The only limitation of this technique is governed by the aperture size, since the aperture will itself diffract. Fig. 3 shows optical diffraction patterns from the same area in the negative using three different aperture sizes. In a, the aperture size is comparable to

0 0 0 0 4 6 0 8 1 7 1

$\sim$35Å in the real crystal. The aperture itself gives diffraction patterns as Fraunhofer rings, which will sometimes interfere with the diffracted spots and broaden the spots. The intensity is low due to the small size of aperture. It is also more difficult to locate the exact center of the diffracted spots as they are broadened and, hence the errors in measurement are increased.

By sacrificing the resolution, a large aperture size gives sharper diffraction spots (Fig. 3b, c) which results in more accurate measurements. Generally, using a rule marked down to 0.5 mm, the estimated accuracy is $\sim$0.5%. This is quite reproducible, the errors originating from uncertainty in measuring the distance between the diffracted spots.

(b) Microdensitometer trace analysis will provide more accurate data as long as there are easily recognizable fringes in the negative. Fig. 4 shows (200) lattice fringes of a pure gold specimen and their corresponding microdensitometer traces. Since the fringes are clear in the micrograph, the microdensitometer trace is also very sharp and the fringe positions can be easily identified as those peaks in the plot.

The exact position of each peak sometimes becomes unidentifiable due to lack of contrast in the negative near the fringe. For example, in the present spinodal alloy, dark and bright diffraction contrast occurs due to the decomposition and this masks the exact position of the fringes. This effect is illustrated in Fig. 5 which shows (200) lattice fringes of Cu-Ni-Cr aged at 600°C for 1 hour and their corresponding microdensitometer traces. The fringe positions become smeared and broadened. This limits the accuracy of measurements.

Hence, in order to minimize these kinds of experimental errors, it is advisable to take an average value over 10 or 20 fringes and thus smooth the curves. Fig. 17 and Fig. 20 are results of averaging over 15 fringes at a time. The accuracy limit is then estimated to be $\sim$1.0%. Nevertheless it is clear for these plots that the interplanar spacing profile can be revealed from such measurements.

(c) Since the lattice fringes broaden at high magnification, it is difficult to locate the exact positions of fringes on the prints. Thus an error always exists for direct measurement from enlarged micrographs. Usually, the accuracy can be improved if measurements averaged over a number of fringes are made. Yet, a reasonable estimation of $\sim$2% error is possible in this method by measuring 10 fringes at a time.

0 0 0 0 4 6 0 8 1 7 2

III. RESULTS

A. The Morphology and Structure of Aged Alloys

The characteristics of spinodal decomposition as observed in the electron microscope are: (1) satellites in the diffraction pattern; (2) modulations in the image.

The as-quenched specimen showed some evidence of segregation in the matrix (Fig. 6). This suggests that the alloy starts decomposing at that condition. Fig. 7 shows a (001) diffraction pattern for alloys aged 10 min. at 700°C. The satellites on either side of the 200 spots along cube directions can be seen from the pattern. This satellite phenomenon arises from a microstructure with fluctuations of composition in a periodic way along <100>.

In spinodally decomposed alloys, the wavelength of the modulations increases with aging time. In Fig. 8, a very fine and wavy microstructure is observed for specimens aged at 700°C for (a) 10 min., (b) 1 hour. As aging continued, the Cu-rich and Cu-poor regions separate into distinct phases (Fig. 9) and become cuboids. Then for still longer aging time (166 hours at 700°C), the cuboids joint together and some of them start to lose coherency (Fig. 10a). Finally, aging for 616 hours at 700°C, interfacial dislocations are created and the two phases become incoherent (Fig. 10b). This sequence is similar to spinodally decomposed Cu-Ni-Fe alloys.[17] By diffraction contrast experiments (using the g•b criterion), it was found that the Burger's vectors of interfacial dislocations are also of the type $\frac{a}{2}$<110> (Fig. 11), as was found in Cu-Ni-Fe alloys.[6,7]

A similar sequence occurs for alloys aged at 600°C (Figs. 12-14), the only difference being that the kinetics of transformation are slower. Thus the two phases remain coherent even after aging as long as 808 hours.

B. Measurements of Decomposition Wavelength

The wavelength of decomposition can be either measured directly from the micrographs, or by calculation from the spacing of satellite spots in the diffraction pattern, using the Daniel-Lipson equation:[18]

$$\lambda = \frac{h \tan \theta}{(h^2 + k^2 + \ell^2)\delta\theta} a_o$$

where θ = Bragg angle for the $(hk\ell)$ reflection in a crystal of lattice parameter a_o, $\delta\theta$ = angular spacing between a satellite spot and its main reflection.

The results are summarized in Table I and Fig. 15 shows the Log-Log plot of aging time versus wavelength. The relation between log λ and log t is linear in the early stages of decomposition and can be represented by $\lambda \propto t^n$, where n is the slope of the Log-Log plot. The values of n are 0.25 for 600°C and 0.32 for 700°C. For longer aging time, the slopes of the curves change and the relatioship between log λ and log t is no longer linear.

C. Lattice Imaging

As mentioned earlier, the high-resolution lattice imaging technique of transmission electron microscopy is utilized in this research to

0 0 0 0 4 6 0 3 1 7 3

detect the lattice parameter difference between the two regions in a spinodally decomposed Cu-Ni-Cr alloy. Fringes on the micrograph result from interference between the transmitted spot and a strongly diffracted spot with periodicity corresponding to the d-spacing of lattice planes in the crystal giving rise to that diffracted spot.

For a perfect crystal, the fringe spacings are identical to the lattice spacings in specimens near the exact Bragg imaging condition. In a crystal with variable d-spacing (as in a spinodal product), the situation is more complex, and the fringe spacings may not directly relate to the actual interplanar spacings in the alloy.[19] However, the measured fringe spacings in the later stages (Table II) in this research have been correlated with previous X-ray data from the two-phase material.[8] The results indicate that the fringe and lattice spacings are identical within experimental error, so that it is reasonable to assume that the same applies to the earlier stages of aging as well.

Therefore, by measuring fringe spacings, the localized lattice parameter of the specimen can be obtained. Since the planar spacings depend on composition, then the lattice imaging method is useful for estimating compositions in the crystal. Thus composition profiles in the material can be shown directly with resolution down to the atomic level by plotting fringe spacing variations versus distance.

(1) Early Stages of Decomposition

In order to detect the compositional fluctuations during the early stages of spinodal decomposition, interplanar spacings, which can be

related to composition, are obtained by directly imaging the lattice planes in the crystal.

Fig. 16 is a lattice imaging micrograph of (200) fringes and its diffraction condition of a specimen aged at 700°C for 10 min. The large-scale dark and bright contrast is due to the composition fluctuations characteristic of a spinodally decomposed product.[4,5] The fringe spacings vary from one region to the other.

Fig. 17 is the corresponding microdensitometer trace analysis of this micrograph averaged over 15 fringe spacings which shows that lattice parameter changes in a periodic manner. The (200) fringe spacing varies from $\sim$1.80 ± 0.025Å (Cu-rich) to 1.78 ± 0.025Å (Cu-poor), which is consistent with the reported results[8] that the lattice constant for the Cu-rich phase is 3.603 ± 0.01Å and 3.571 ± 0.002Å for the Cu-poor phase. These also have been confirmed by X-ray analysis of this alloy. The average wavelength from Fig. 17 is approximately 48 ± 8Å, which is very close to that measured directly on enlarged micrographs (65 ± 5Å) and indirectly from the satellite spacings (50 ± 5Å) (Table I). Measurement of fringe spacings by optical diffraction (using an aperture size about 55Å) gives similar results (Fig. 18) indicating that lattice parameter changes in a sinusoidal manner.

Similarly, lattice images of alloys aged at 600°C for 1 hour (Fig. 19) also provide information about wavelengths and difference in lattice parameter both by microdensitometer analysis (Fig. 20) and by optical diffraction (Fig. 21).

Table II contains the summarized results of (200) fringe spacings obtained by the three different methods. For early stages, Δa varies

0 0 0 0 4 6 3 8 1 7 4

with a short wavelength periodicity and the values appeared in this table are estimates averaging over at least 100 fringe spacings. For the later stages, values are obtained by measuring fringe spacings in purely Cu-rich or Cu-poor region. These results are in accordance with X-ray analysis.

(2) Later Stages of Decomposition

For later stages of aging, two distinct regions corresponding to Cu-rich (the matrix with larger lattice constant) and Cu-poor (the particles with smaller lattice constant) are present in the material. Measurements of (200) lattice fringe spacings from the two regions can readily show the difference.

Fig. 22 is the (200) lattice imaging micrograph of the alloy aged at 600°C for 808 hours. A series of optical diffraction patterns with aperture size about 120Å in the real crystal were taken from this area, each one corresponding to the region marked with the appropriate letter on the micrograph. Fig. 23 shows the lattice parameters calculated from these patterns. There is almost exact correspondence in lattice parameter obtained from optical diffraction patterns and by X-ray analysis. The data also prove that the matrix is Cu-rich of bright contrast region and has larger lattice parameter, while the particles are Cu-poor of dark contrast region with smaller lattice parameter (as expected from volume fraction considerations).

Interesting features of this series of diffraction patterns are shown as the aperture is place around the interface between the two phases. Then the optical diffraction pattern shows two diffracted spots

(in D, G, K, L of Fig. 22) which result from diffraction from the two phases in which the lattice parameters are different.

Satellite spots are observed from area C in Fig. 22 and this suggests that a certain periodicity exists in that area. For a refined analysis of this area, a further series of optical diffraction patterns were taken (Fig. 24) which reveal that the lattice is continuous from one phase to the other. At the interface, expansion and contraction of the lattices occur which result in a greater separation of the diffraction spots. This effect is also confirmed by the direct microdensitometer measurements. These indicate that abnormally large and small d-spacings are present at the interface, which may result from: a) lattice strains; b) unusual composition profile; c) some electron optical effect.

At present this observation is not fully understood, but it has important implications in interpreting fringe spacings near precipitate and matrix interfaces, and this aspect will be investigated further in future work.

Similar results are obtained for alloys aged at 700°C for 166 hours. Fig. 25 shows the (200) lattice fringes and optical diffraction patterns (aperture size around 120Å) which reveal the characteristics of the two phases.

When aging at 600°C, the particles are coherent with the matrix. Fig. 26 is a micrograph of alloys aged at 600°C for 808 hours. At the interface, the fringes are continuous from the Cu-poor region to the Cu-rich region, suggesting that the two regions are still coherent. This provides a direct observation of interfacial microstructure in the

0 0 0 3 4 6 0 8 1 7 5

material and it can be achieved only by utilizing such high-resolution techniques as lattice imaging.

D. Mechanical Tests

The results of the tensile tests are summarized in Table III. For alloys aged at 700°C, the yield stress remains almost constant between aging times as short as 10 min. and as long as 50 hours. It then decreases for longer aging times. For alloys aged at 600°C, the yield stress increases with aging time and then remains constant (Fig. 27).

Fractography reveals that the as-quenched and the specimen aged 10 min. at 700°C fractured in a ductile manner (Fig. 28a). The mode of failure then became intergrannular, with some small regions of ductile failure after longer aging times (Fig. 28b).

Similarly when the alloy was aged at 600°C, this kind of transition from ductility to brittleness was also observed. This is similar to the behavior of Cu-Ni-Fe.[7]

IV. DISCUSSION

A. Morphologies of the Phases

The rates of spinodal decomposition at high temperature (700°C) and low temperature (600°C) were found to be different. When aging at 700°C, the decomposition is fast. From the data we believe that the whole alloy takes less than 10 min. to complete the transformation since the lattice parameters of the two regions remained almost constant after aging 10 min. (Table II). The same situation occurs for alloys aged at 600°C. Due to small differences in lattice parameters between the two regions, it is very difficult to say how long it takes to complete the whole decomposition.

The as-quenched specimen showed some sign of precipitates in the matrix (Fig. 6). Badia, Kirby, and Mihalisin[9] in studying the strengthening of Cu-Ni-Cr alloys found that precipitation of an almost pure chromium phase took place in the as-quenched specimens. But here in this research, no evidence for this has been found. Presumably quenching was sufficiently fast to prevent such a possible reaction.

As decomposition proceeds when aging at high temperature (700°C), a second phase precipitates out from the matrix. The two phases are initially coherent. The wavy appearance of the particles during the early stages of decomposition (Fig. 8) can be understood qualitatively by considering the changes in microstructure. Livak[20] made an analysis in a Cu-Ni-Fe spinodal alloy and concluded that this wavy appearance is due to the fact that during the early stages of decomposition, the matrix is partially decomposed and the microstructure consists

0 0 : 0 4 0 0 8 1 7 6

of a multi-dimensional distribution of particles. The particle morphology was transforming to a one-dimensional distribution and no preferred (100) habit is developed until the equilibrium tie-lines were reached. Consequently, the microstructure had a wavy appearance as observed in the electron micrographs.

The present alloy is a Cu-rich material. So as the second phase precipitates out from the matrix, this phase is Ni-Cr-rich, or Cu-poor. In the electron microscope, the two phases show bright and dark contrast. Cadoret and Delavignette[21] studied the contrast in the electron microscope of spinodally decomposed Cu-Ni-Fe alloys and concluded that the contrast results from atomic displacements in the direction of the composition fluctuations or waves. This is confirmed by the lattice imaging technique which shows that the bright region corresponds to the larger lattice parameter area characteristic of Cu-rich phase, while dark regions correspond to the Cu-poor phase.

As soon as the decomposition reaches the equilibrium tie-line, particle coarsening becomes obvious. A log-log plot of wavelength versus aging time gave $\lambda \sim Kt^{0.32}$ for 700°C, and $\lambda \sim Kt^{0.25}$ for 600°C. This is pretty close to $\lambda \sim Kt^{1/3}$, which is consistent with the theories of diffusion controlled coarsening in which large particles grow at the expense of small ones.

For aging over 166 hours at 700°C, loss of coherency of the particles was observed (Fig. 7). This is because of the large size of the particles ($\lambda \sim 1000\text{Å}$) and in order to decrease the strain energy between the two phases, interfacial dislocations are created. For aging at 600°C, particles remain coherent even after aging as long as 808 hours.

B. Correlations of Microstructures and Mechanical Properties

From the tensile test results of this research, the yield stress of the spinodally decomposed alloys increased with longer aging time until the equilibrium tie-line compositions were reached. Dahlgren[11] has calculated the yield stress of alloys with coherent lamellar microstructures and his theory is based on the elastic strains required to maintain coherency between the two phases. The conclusions reached by Dahlgren in his calculations are that the yield stress of spinodally decomposed Cu-Ni-Fe alloys depends on the difference in cubic lattice parameters of the two phases, and is independent of the wavelength and of the volume fractions of the precipitating phases between certain critical values. Butler and Thomas[6] and Livak and Thomas[19] have proved Dahlgren's theory by studying symmetric and asymmetric Cu-Ni-Fe alloys. They used Curie temperature measurements to obtain composition profiles in the specimen and correlated these with lattice parameter changes. Then they found that the increase in yield stress is linearly proportional to the lattice parameter's difference of the two phases.

The physical basis for Dahlgren's calculations was the same one as used by Mott and Nabarro[22] to derive the following expression for the average internal stress due to spherical, coherent precipitates,

$$\sigma_i \sim 2G\varepsilon f$$

where G is the average shear modulus, ε is the misfit parameter between solute and solvent atoms, and f is the volume fraction of the precipitating phase.

0 0 0 0 4 6 0 8 1 7 7

Cahn[23] found that the yield stress of spinodal alloys should be proportional to the product of the amplitude (A) squared and the wavelength (λ) of the composition modulation, $A^2\lambda$, based on the resistance to dislocation motion being due to a Mott-Nabarro type barrier. But Ditchek and Schwartz[24] found that this has not been consistently observed by studying Cu-Ti and Cu-Ni-Fe alloys. Then they proposed a new mechanism of hardening for spinodal alloys. The model is based on a calculation of the shear stress due to misfit strains caused by the passage of a dislocation on its slip plane. The yield stress increment was thus found to be proportional to $(A/\lambda)S$, where A is the amplitude of the compositional fluctuations, S is a "squaring factor," and when S was substituted by $(\lambda - \lambda_o)$, where λ_o is the fundamental wavelength of decomposition, a plot of ΔY.S. versus $(A/\lambda)(\lambda - \lambda_o)$ shows a linear relationship. Hence, these researchers concluded that S is proportional to $(\lambda - \lambda_o)$. For short aging times, the yield stress increment rises rapidly due to the rapid rise in $(\lambda - \lambda_o)/\lambda$. In the later stages, $(\lambda - \lambda_o)/\lambda$ nears unity and ΔY.S. $\propto$ A, which is exactly Dahlgren's argument.

For the present Cu-Ni-Cr alloy, the mechanical behavior is much the same as that of Cu-Ni-Fe alloys. When aged at 700°C, the yield stress does not change much between 10 min. and 50 hours. The reason for this may be due to the fact that decomposition has been completed even before 10 min. as suggested from the lattice parameter measurements (Table II).

The explanation for the decrease in yield stress for still longer aging times may be due to the large wavelength in the microstructure and the fact that the particles begin to lose coherency. The strengthening

of the coherent microstructure in decomposed Cu-Ni-Cr alloys arises from the difference in the lattice parameters and also the shear moduli of the two phases. When the particles became semi-coherent, the coherency strains are relieved and thus the yield stress is reduced.

Livak[17] has studied loss of coherency in Cu-Ni-Fe alloys and concluded that when coherency is lost, the strengthening is due to the difference in shear moduli and also to the interfacial dislocations. When the particles are coherent (λ small), a dislocation will encounter many obstacles as it glides through this structure under an applied stress. But when particles are very large, the interface encountered by a slip dislocation becomes more like that in the lamellar microstructure of the directional solidified eutectic alloys in which it has been observed that yield stress is proportional to $\lambda^{-1/2}$.

The decrease in yield stress of Cu-Ni-Cr alloy occurred when the particles began to lose coherency (Fig. 10). Also, it is found by light optical metallography that discontinuous coarsening along grain boundaries are observed at that aging time (Fig. 29). The fractography results showed intergranular fracture (Fig. 28b). This suggests that the fracture stress of the grain boundaries is less than that of the matrix and the fracture stress of the grain boundaries is reached before the matrix failed. This discontinuous coarsening along the grain boundaries results also in the decrease of the ultimate tensile stress (Table III).

The yield stress increases as aging time increases for alloys aged at 600°C (Table III). Fig. 30 shows a plot of ΔY.S. versus the difference in lattice parameters of the two phases. From the above

0 0 3 0 4 6 3 8 1 7 8

discussion, any definite correlation between the mechanical properties and microstructure can be seen to depend on the compositional fluctuations. But in this research, the compositional fluctuations, or Δa, show only $\sim$1% difference between the two phases and the experimental error is estimated to be around 1/2% to 1%. So it is inadequate to justify whether Dahlgren's theory or Ditchek and Schwartz's correction is more applicable from the results in this research. Yet at least there seems to be a dependence of yield stress increment on the lattice parameter differences (Fig. 30).

V. CONCLUSIONS

From this high-resolution electron microscopy study of spinodally decomposed Cu-Ni-Cr alloy, the following conclusions are obtained:

(1) This material behaves spinodally like that of Cu-Ni-Fe alloys. As aging proceeds, coarsening of particles occurs which obeys the law $\lambda \propto t^n$, where $n \sim \frac{1}{3}$ at 700°C, $n \sim \frac{1}{4}$ at 600°C.

(2) Loss of coherency is observed for alloys aged at 700°C after 166 hours. Interfacial dislocations with Burger's vector of $\frac{a}{2}$ <110> type are created. The yield stress is observed to decrease at that aging condition.

(3) High-resolution lattice imaging technique has proved to be able to detect lattice parameter changes between the two phases even when the maximum difference is only ~1%.

The significance of this fundamental work in the interpretation of fringe spacings is important for future research in detecting small lattice parameter differences. It proves the capability of lattice imaging in resolving 1% lattice parameters difference in alloys and lays the foundation for future applications to other metallurgical systems.

(4) From fringe spacings analysis, Cu-rich region with lattice constant 3.60 ± 0.02Å and Cu-poor region with lattice constant 3.56 ± 0.02Å are found which are consistent with previous studies by X-ray methods. Interesting features about interfaces are revealed through this lattice imaging technique and it suggests that there are other microstructural details down to atomic levels which can be observed by this technique.

0 0 3 0 4 6 0 8 1 7 9

(5) A drop in yield stress after aging at 700°C for 166 hours is observed and is a result of relieving strain when particles begin to lose coherency.

(6) Due to the fact that $(\Delta a)_{max}$ is too small in this system, the correlation between mechanical properties and microstructure is not unambiguous. That there is a dependence of the increment of yield stress on Δa can be indicated from the results.

ACKNOWLEDGEMENTS

The author wishes to express his gratitude to Professor Gareth Thomas for his guidance in this research. Appreciation is also extended to Dr. Robert Sinclair for his assistance in experiment and critical review of the manuscript. Many helpful discussions with other members of the electron microscopy group in the Materials Science Department at Berkeley are also acknowledged.

Love and encouragements from the author's family members, such as his parents (Mr. and Mrs. F. S. Wu), his brother (Dr. Wei-Kuo Wu), and, of course, his wife, Sophia, are highly appreciated. Without their help the author is just impossible to be able to study here in Berkeley.

This work was supported by the U.S. Energy Research and Development Administration through the Materials and Molecular Research Division of the Lawrence Berkeley Laboratory, Berkeley, California.

0 0 0 0 4 6 9 3 1 8 0

REFERENCES

1. Reports on "Cu-Ni alloy IN-732" from International Nickel Company, Inc. (1969).
2. The Scientific Papers of Williard Gibbs (Dober, 1961), p. 105.
3. M. Hillert, Acta Met., 9, 525 (1961).
4. J. W. Cahn, Acta Met., 9, 795 (1961).
5. J. W. Cahn, Acta Met., 10, 179 (1962).
6. E. P. Butler and G. Thomas, Acta Met., 18, 347 (1970).
7. R. Livak and G. Thomas, Acta Met., 19, 497 (1971).
8. J. L. Meijering, G. W. Rathenau, M. G. van der Steeg, and P. B. Braun, J. Inst. Metals, 84, 118 (1955-1956).
9. F. A. Badia, G. N. Kirby, and J. R. Mihalisin, Trans. ASM, 60, 395 (1967).
10. E. L. Huston, J. W. Cahn, and J. E. Hilliard, Acta Met., 14, 1053 (1966).
11. S. D. Dahlgren, Ph.D. Thesis, University of California, UCRL-16846 (1966).
12. G. Thomas, Transmission Electron Microscopy of Metals (John Wiley & Sons, New York, 1961).
13. J. G. Allpress and J. V. Sanders, J. of Applied Cryst., 6, 165 (1973).
14. R. Sinclair, K. Schneider, and G. Thomas, Acta Met., 23, 873 (1975).
15. R. Gronsky, M. Okada, R. Sinclair, and G. Thomas, EMSA (1975), p. 22.
16. R. Sinclair, R. Gronsky, and G. Thomas, Acta Met., 24, 789 (1976).
17. R. J. Livak, Ph.D. Thesis, University of California, Berkeley, LBL-1107 (1972).

18. V. Daniel and H. Lipson, Proc. Roy. Soc., 182, 378 (1943).

19. D. J. H. Cockayne, EMSA (1975), p. 2.

20. R. J. Livak, M.S. Thesis, University of California, Berkeley, UCRL-19189 (1970).

21. R. Cadoret and P. Delavignette, Physics Stat. Sol., 35, 119 (1969).

22. N. F. Mott and F. R. Nabarro, Proc. Roy. Soc., 52, 86 (1940).

23. J. W. Cahn, Acta Met., 11, 1275 (1963).

24. B. Ditchek and L. H. Schwartz, in press.

Table I. Measurements of Wavelength

(A) 700°C

Aging Time	10 min.	1 hour	71 hrs.	125 hrs.	166 hrs.	616 hrs.
Measured from Diff. Pattern	50 ± 5Å	114 ± 5Å	--	--	--	--
Measured from Micrograph	65 ± 5Å	120 ± 8Å	430 ± 7Å	661 ± 10Å	979 ± 10Å	~2000Å

(B) 600°C

Aging Time	10 min.	30 min.	1 hour	20 hrs.	405 hrs.	808 hrs.
Measured from Diff. Pattern	45 ± 5Å	--	105 ± 5Å	215 ± 5Å	--	--
Measured from Micrograph	70 ± 10Å	110 ± 8Å	115 ± 10Å	234 ± 8Å	483 ± 10Å	869 ± 9Å

Table II. Fringe Spacing Measurements

(A) 700°C

Aging Time	Region	Direct Measurement from Micrograph	Microdensitometer	Optical Diffraction
10 min.	Cu-Rich	3.60 ± 0.1Å	3.60 ± 0.05Å	3.60 ± 0.02Å
	Cu-Poor	3.56 ± 0.1Å	3.56 ± 0.05Å	3.56 ± 0.02Å
166 hours	Cu-Rich	3.60 ± 0.1Å	3.61 ± 0.05Å	3.60 ± 0.02Å
	Cu-Poor	3.55 ± 0.1Å	3.56 ± 0.05Å	3.55 ± 0.02Å

(B) 600°C

Aging Time	Region	Direct Measurement from Micrograph	Microdensitometer	Optical Diffraction
1 hour	Cu-Rich	3.60 ± 0.1Å	3.60 ± 0.05Å	3.59 ± 0.02Å
	Cu-Poor	3.56 ± 0.1Å	3.57 ± 0.05Å	3.57 ± 0.02Å
808 hours	Cu-Rich	3.61 ± 0.1Å	3.61 ± 0.05Å	3.60 ± 0.02Å
	Cu-Poor	3.56 ± 0.1Å	3.55 ± 0.05Å	3.55 ± 0.02Å

Table III. Tensile Test Results

(A) 700°C

Aging Time	As Quenched	10 min.	1 hr.	50 hrs.	166 hrs.	616 hrs.
Yield Stress (KSI)	22.5	41.1	42.3	42.1	36.3	34.6
Ultimate Tensile Stress (KSI)	51.0	56.8	64.4	61.2	53.2	56.7
Elongation	--	5.4%	18.1%	11.7%	--	--

(B) 600°C

Aging Time	As Quenched	10 min.	1 hr.	50 hrs.	360 hrs.	616 hrs.
Yield Stress (KSI)	22.5	29.6	37.9	48.6	51.4	49.6
Ultimate Tensile Stress (KSI)	51.0	57.4	58.3	61.1	66.5	65.3
Elongation	--	24.7%	15.9%	8.1%	9.6%	7.3%

FIGURE CAPTIONS

Fig. 1. Ni-Cr-Cu ternary phase diagram at 930°C. A: homogeneous b.c.c.; B: homogeneous f.c.c.; C: 2 f.c.c. phases; D: b.c.c. and Cu-Rich f.c.c.; E: b.c.c. and Ni-rich f.c.c.; F: b.c.c. and 2 f.c.c. phases.

Fig. 2. Dimension of tensile specimens.

Fig. 3. Optical diffraction patterns taken from same area with different aperture size. (a) $\sim$35Å, (b) $\sim$55Å, (c) $\sim$120Å.

Fig. 4. Microdensitometer traces of Au (200) fringes.

Fig. 5. Microdensitometer traces of Cu-Ni-Cr (200) fringes after aging at 600°C for 1 hour.

Fig. 6. Transmission electron micrograph of as-quenched specimen (a) and its diffraction pattern (b).

Fig. 7. (001) diffraction pattern of specimen aged at 700°C for 10 min. Satellite spots can be seen along cube directions from <200> spots.

Fig. 8. Transmission electron micrograph of alloy aged at 700°C for (a) 10 min. (b) 1 hour.

Fig. 9. Transmission electron micrograph of alloy aged at 700°C for (a) 71 hours (b) 125 hours.

Fig. 10. Transmission electron micrograph of alloy aged at 700°C for (a) 166 hours (b) 616 hours. Note that at this stage particles begin to lose coherency.

0 0 0 0 4 6 0 0 1 0 3

Fig. 11. Electron diffraction contrast experiment to determine the Burger's vectors of interfacial dislocations by using g•b criterion for alloy aged at 700°C for 616 hours. (a) g = $[\bar{2}00]$; (b) g = [220]; (c) g = [020]; (d) g = $[\bar{2}20]$.

Fig. 12. Micrograph of alloy aged at 600°C for (a) 10 min. (b) 30 min.

Fig. 13. Electron micrograph of alloy aged at 600°C for (a) 1 hour; (b) 20 hours.

Fig. 14. Electron micrograph of alloy aged at 600°C for (a) 405 hours; (b) 808 hours.

Fig. 15. Plot of log (wavelength) versus log (aging time) for alloys aged at 600°C and 700°C.

Fig. 16. (200) lattice imaging micrograph of alloy aged at 700°C for 10 min. and its corresponding diffraction pattern. d_1 is the fringe spacing of Cu-rich (bright) region while d_2 is Cu-poor (dark) region.

Fig. 17. Microddensitometer trace analysis of Fig. 16. Note that fringe spacings change in a periodic manner and λ calculated from this plot is $\sim 48 \pm 8$ Å.

Fig. 18. Optical diffraction results of Fig. 16, indicating also that fringe spacings change in a periodic way.

Fig. 19. (200) lattice imaging micrograph of alloy aged at 600°C for 1 hour and its corresponding diffraction pattern. d_1 is fringe spacing of Cu-rich (bright) region while d_2 is that of Cu-poor (dark) region.

Fig. 20. Microdensitometer trace analysis of Fig. 19, revealing that fringe spacings change in a periodic manner and wavelength calculated from this plot is $\sim$100 $\pm$ 6Å.

Fig. 21. Optical diffraction results of Fig. 19, showing that fringe spacings change in a sinusoidal manner.

Fig. 22. (200) lattice imaging micrograph of alloy aged at 600°C for 808 hours and optical diffraction patterns (aperture size $\sim$120Å) taken from this same micrograph, each one corresponding to the region marked with the appropriate letter on the micrograph. Satellite spots can be seen in (c), two diffracted spots can be seen in D, G, K, L.

Fig. 23. Optical diffraction results of Fig. 22, showing the characteristics of the two phases by larger (Cu-rich) and smaller (Cu-poor) fringe spacings.

Fig. 24. (200) lattice imaging micrograph of alloy aged at 600°C for 808 hours and corresponding optical diffraction patterns (with aperture size $\sim$120Å) taken from the same micrograph. Note around the interface, satellite spots can be seen and abnormal larger and smaller fringe spacings are observed at the interface.

Fig. 25. (200) lattice imaging micrograph of alloy aged at 700°C for 166 hours and optical diffraction patterns (with aperture size $\sim$120Å) taken from Cu-rich phase, Cu-poor phase, and at the interface.

0 0 0 0 4 6 0 3 1 8 4

Fig. 26. (200) lattice imaging micrograph of alloy aged at 600°C for 808 hours. Note that the fringes are continuous from Cu-poor phase to Cu-rich phase, showing that the two phases are still coherent.

Fig. 27. Plot of yield stress versus log (aging time) for alloys aged at 600°C and 700°C.

Fig. 28. Scanning electron fractograph of alloy aged at 700°C for (a) 10 min. (b) 616 hours, showing the change from ductile failure to intergranular failure.

Fig. 29. Optical micrographs of alloy aged at 700°C for 166 hours, showing that discontinuous coarsening along grain boundaries is observed [(a)-(d)].

Fig. 30. Plot of Δ (yield stress) versus Δ (lattice parameter), indicating the dependence of Δ(Y.S.) on Δa.

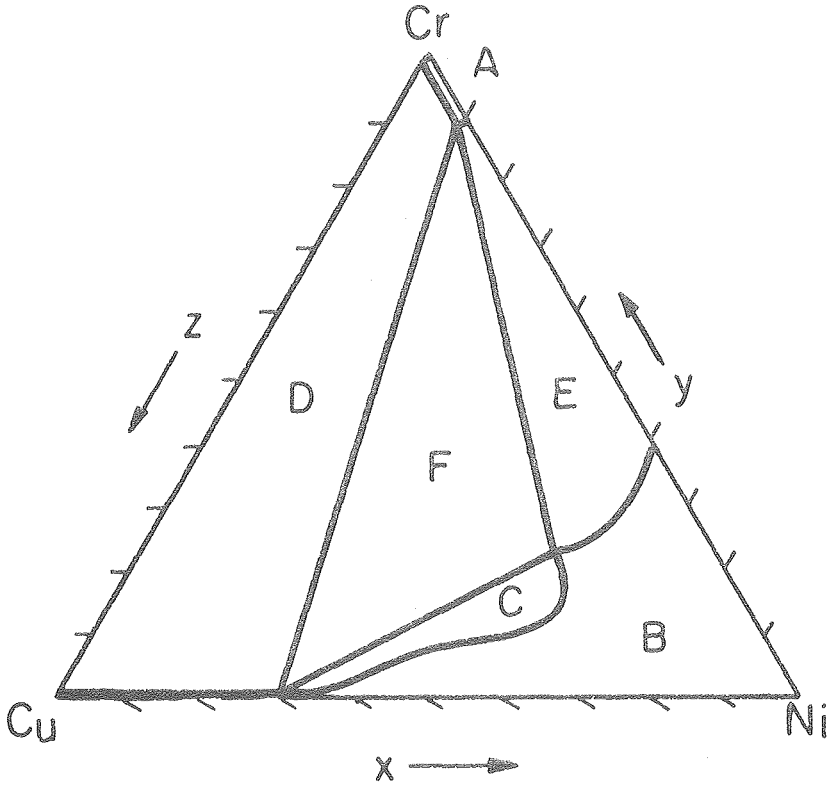

XBL7611-7704

Fig. 1

0 0 0 0 4 6 0 6 1 8 5

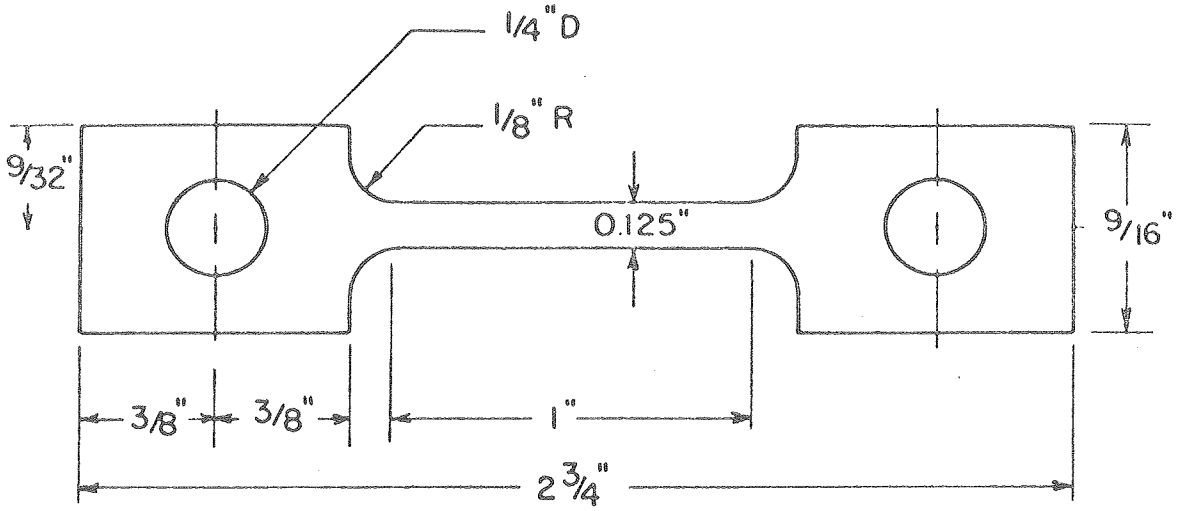

GAGE LENGTH: 1"

TENSILE SPECIMEN

XBL 705-911

Fig. 2

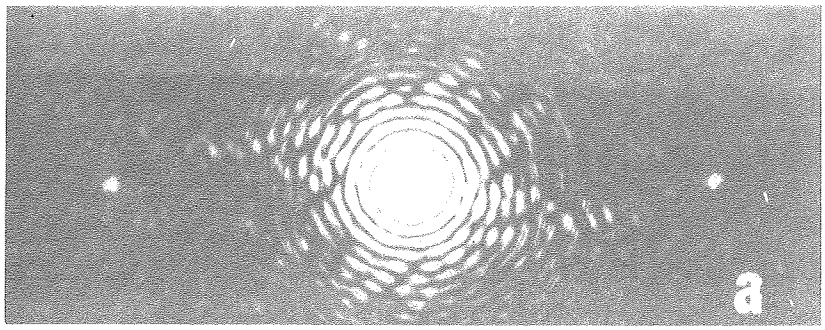

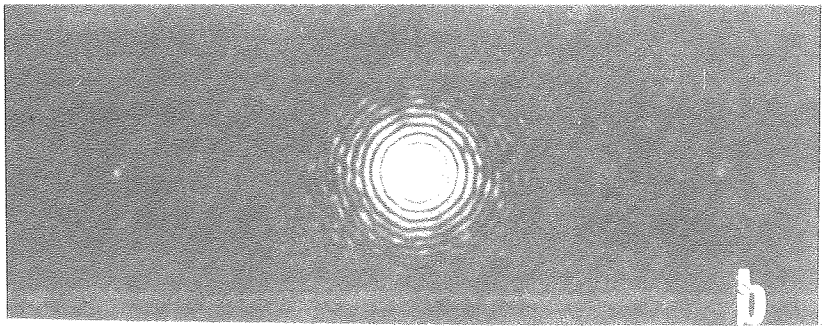

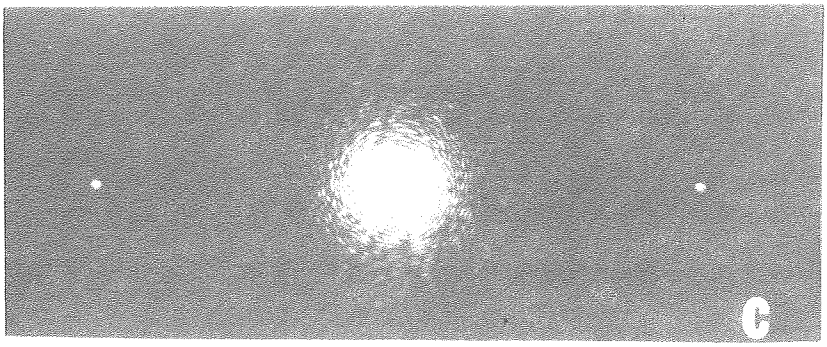

XBB760-10144

Fig. 3

0 0 0 0 4 6 3 6 1 8 6

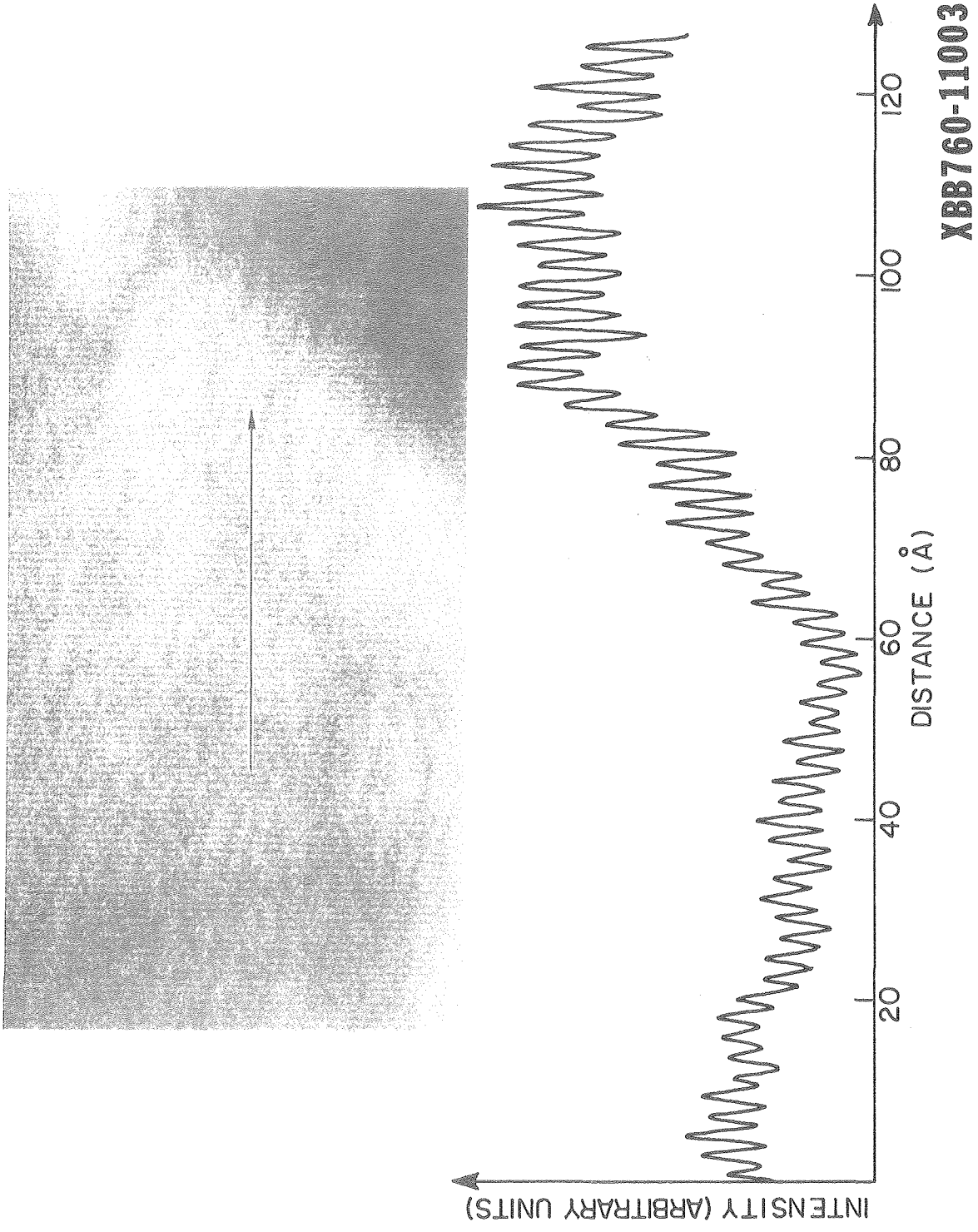

Fig. 4.

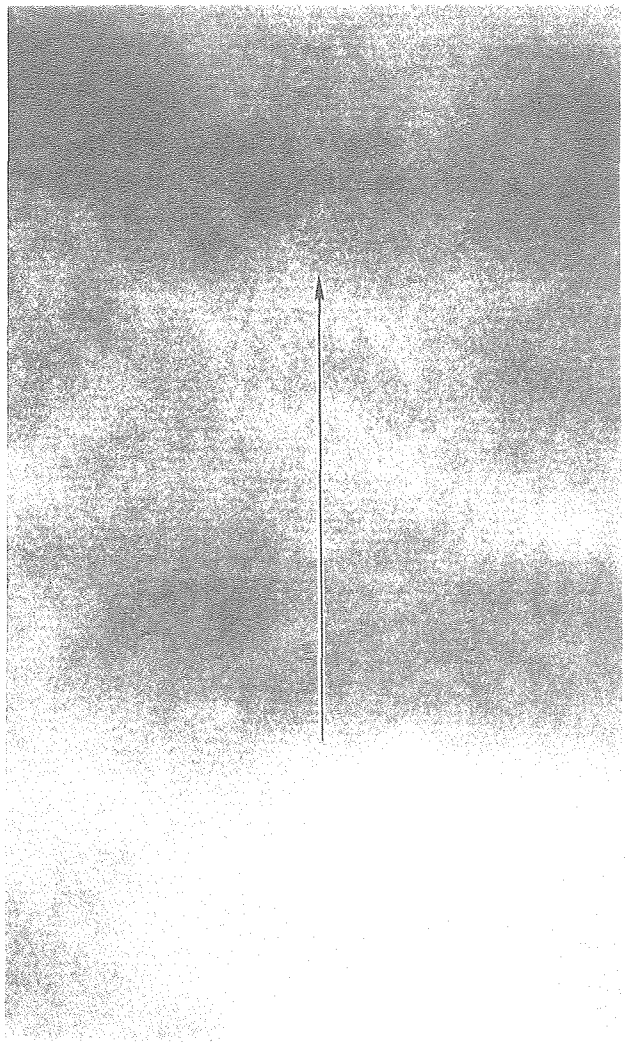

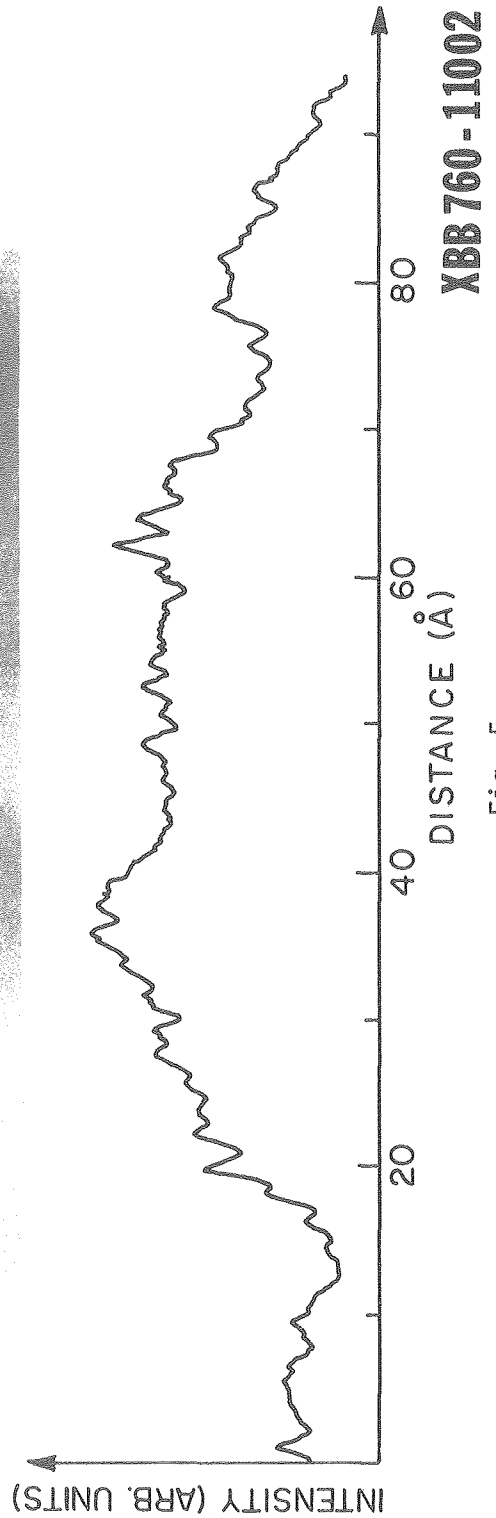

Fig. 5

0 0 0 3 4 6 0 8 1 8 7

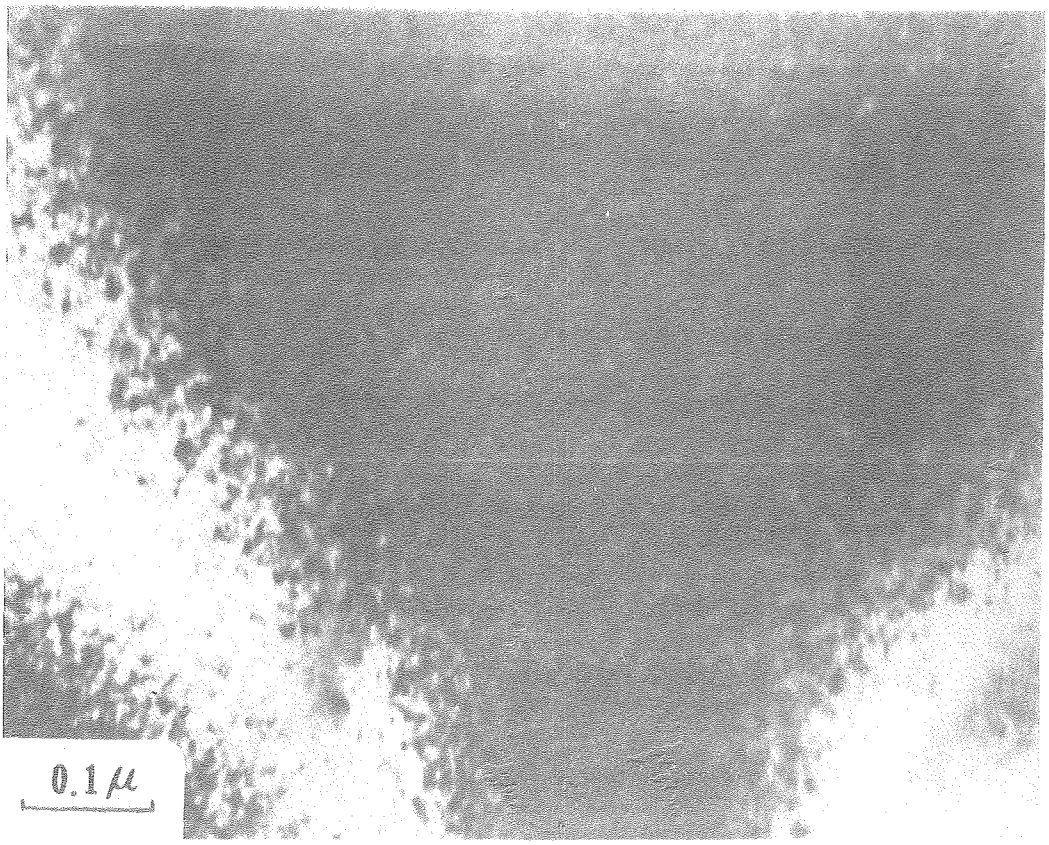

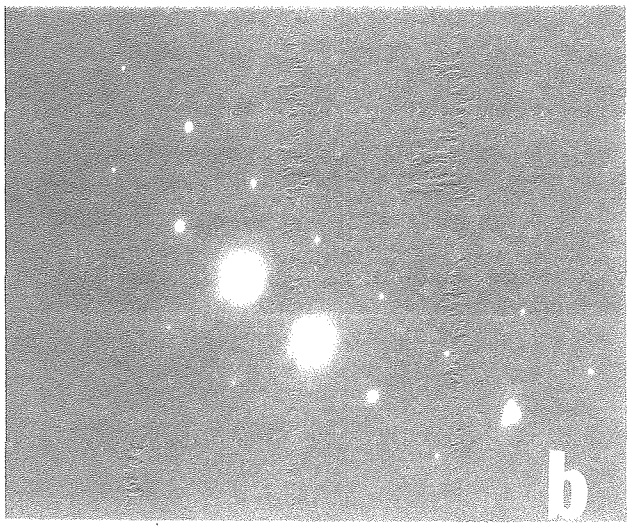

XBB 760-10142

Fig.6

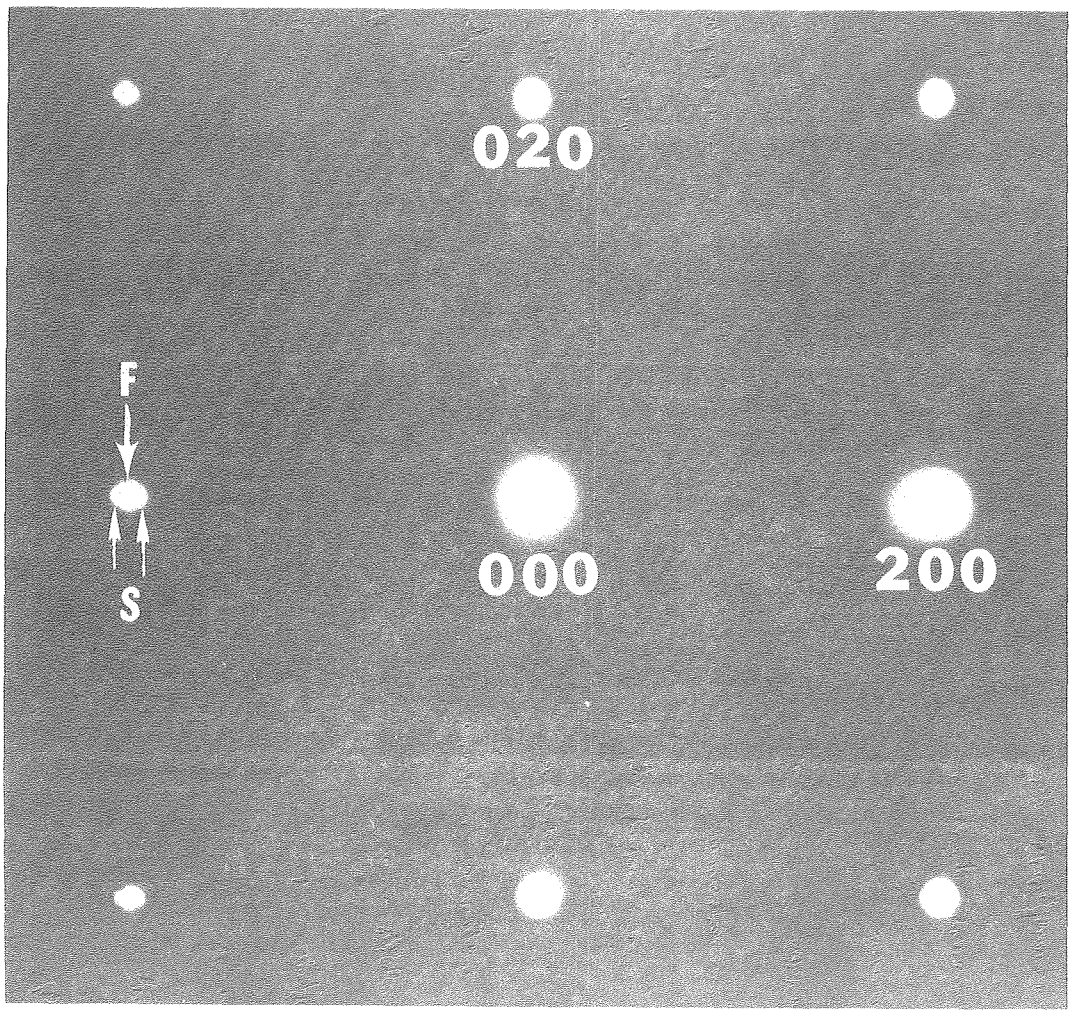

XBB 760-10143

Fig. 7

0 0 0 3 4 6 0 6 1 3 8

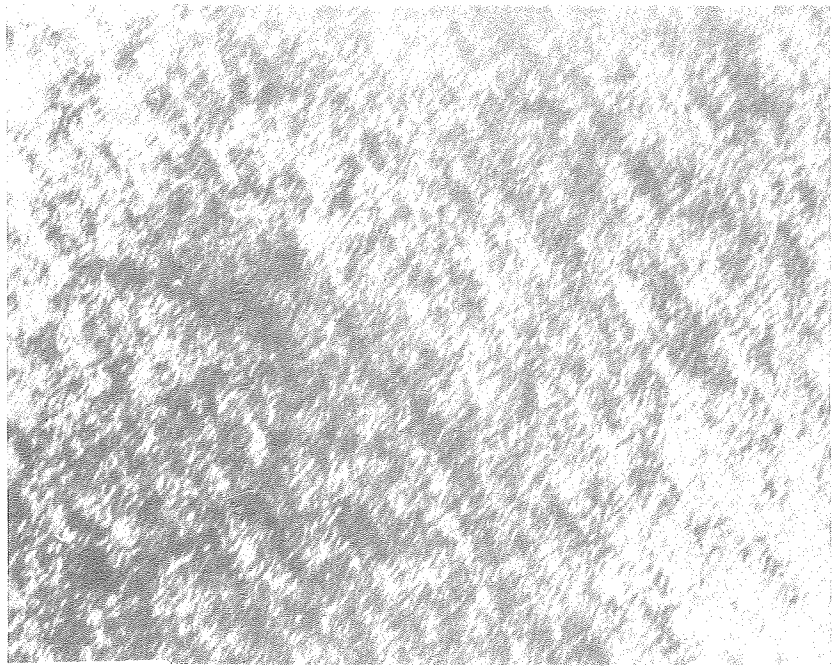

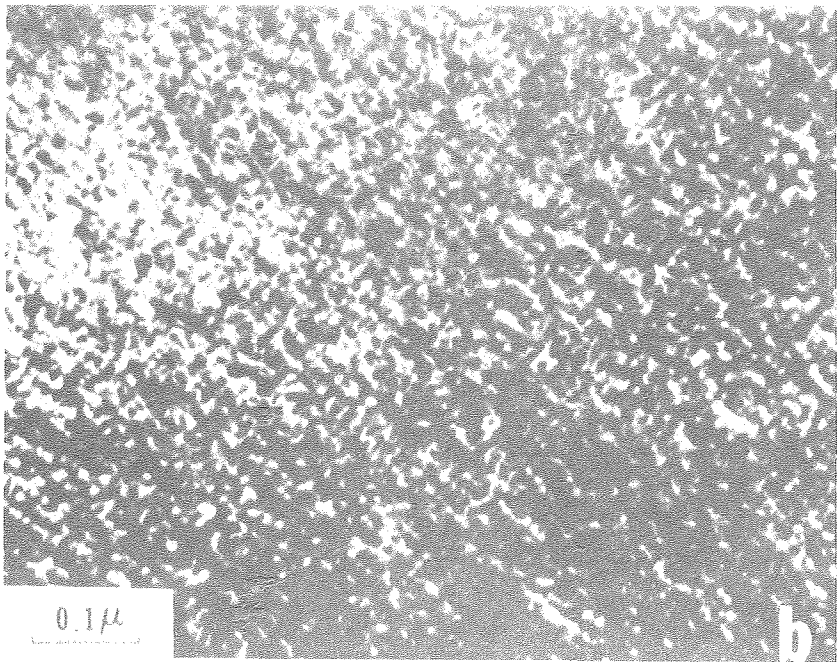

XBB760-10140

Fig. 8.

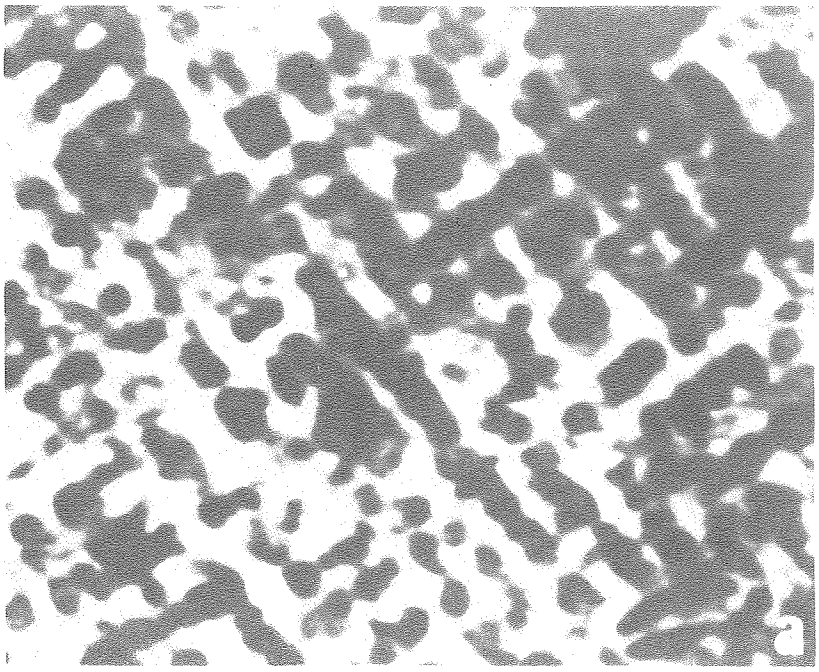

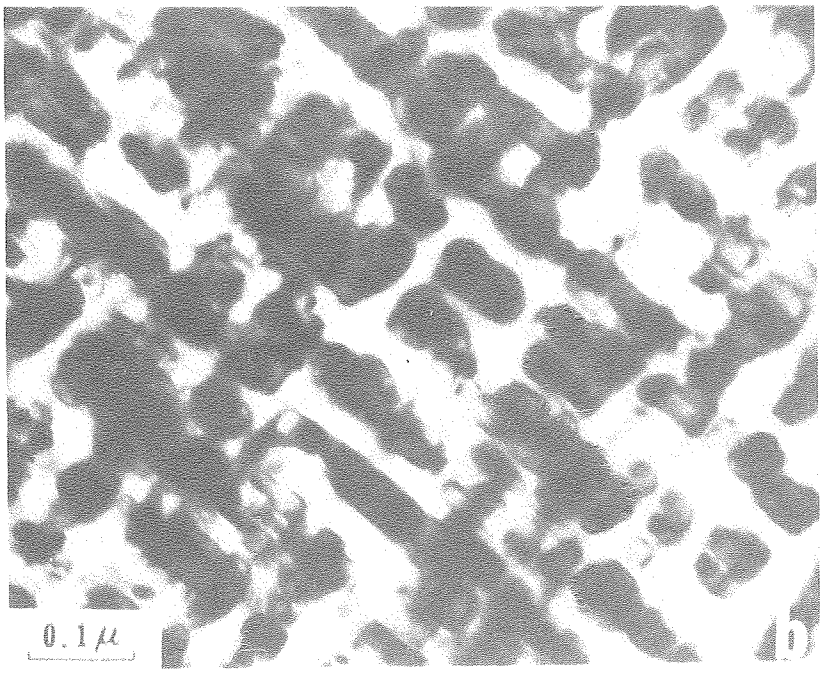

Fig. 9 XBB 760-10138

0 0 0 0 4 6 0 3 1 8 9

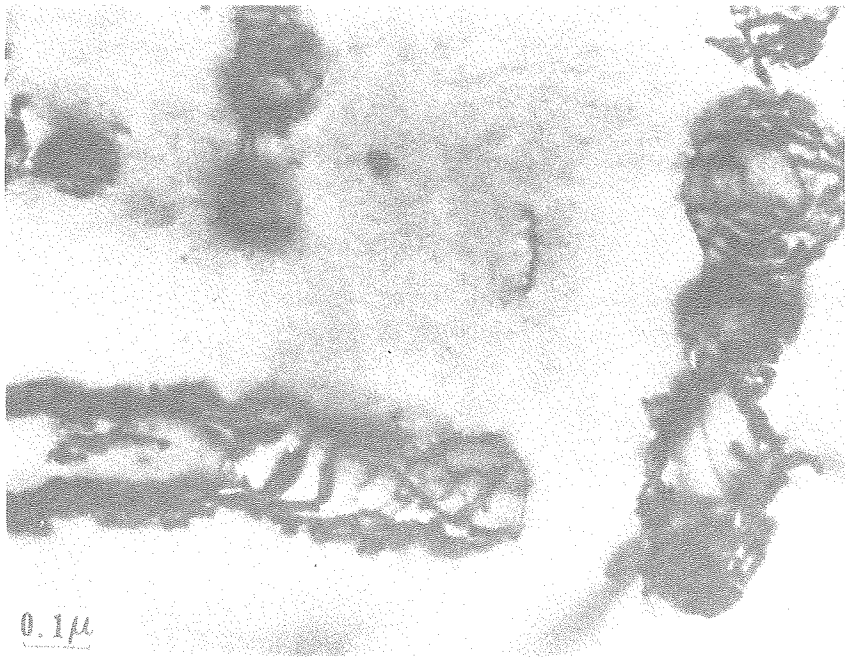

XBB760-10128

Fig.10

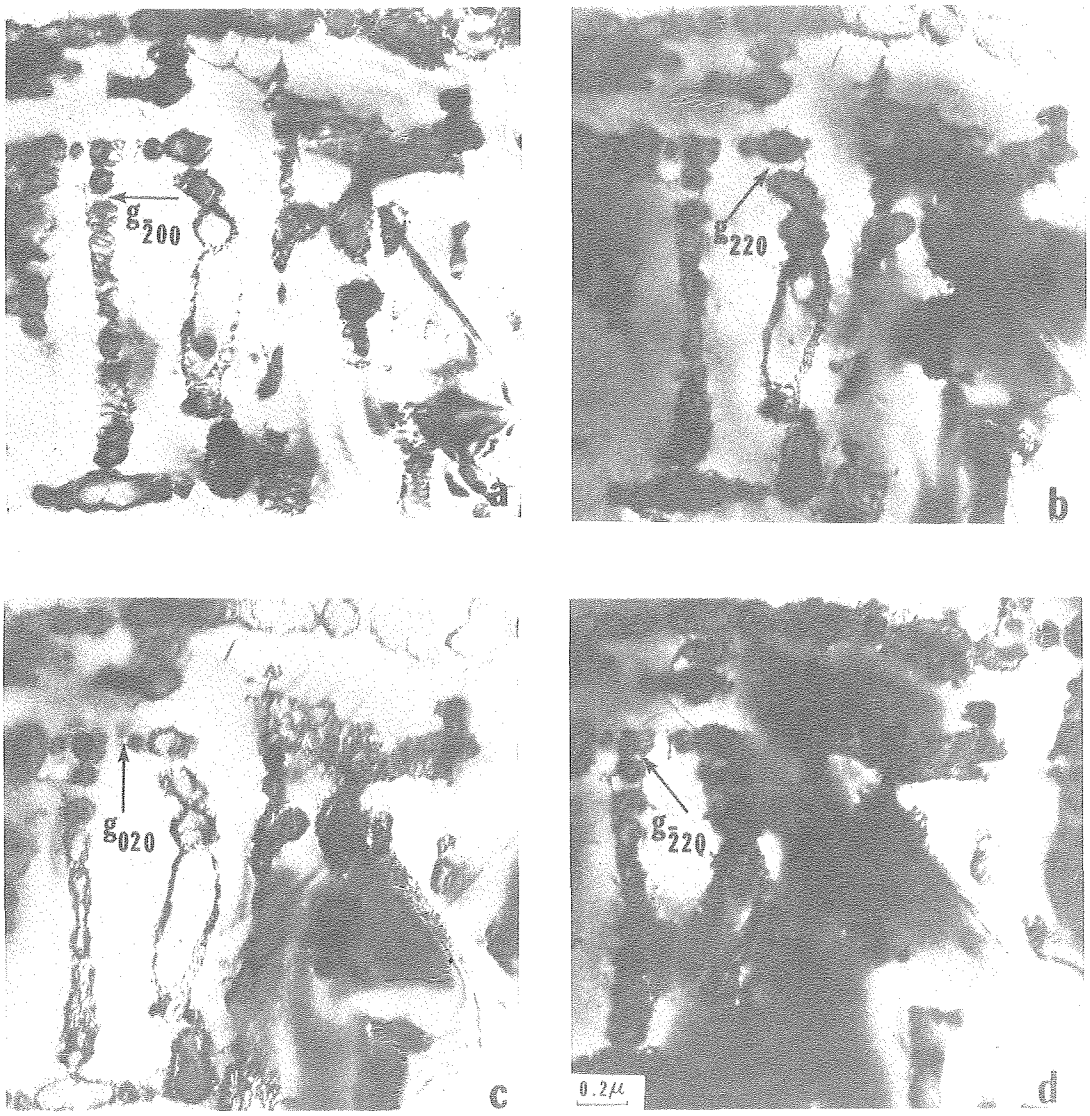

XBB 760-10127

Fig. 11

0 0 0 0 3 4 6 3 8 1 9 0

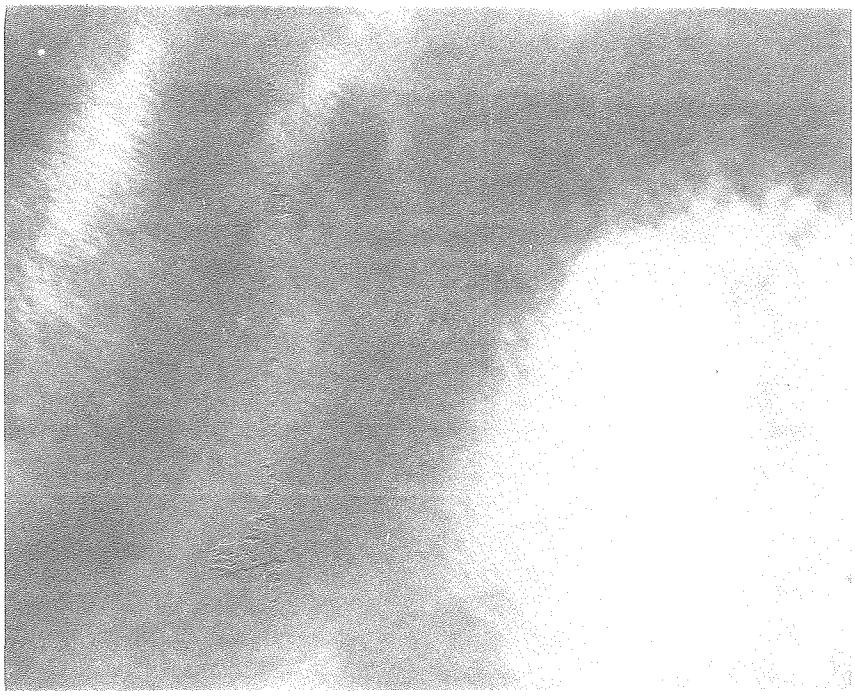

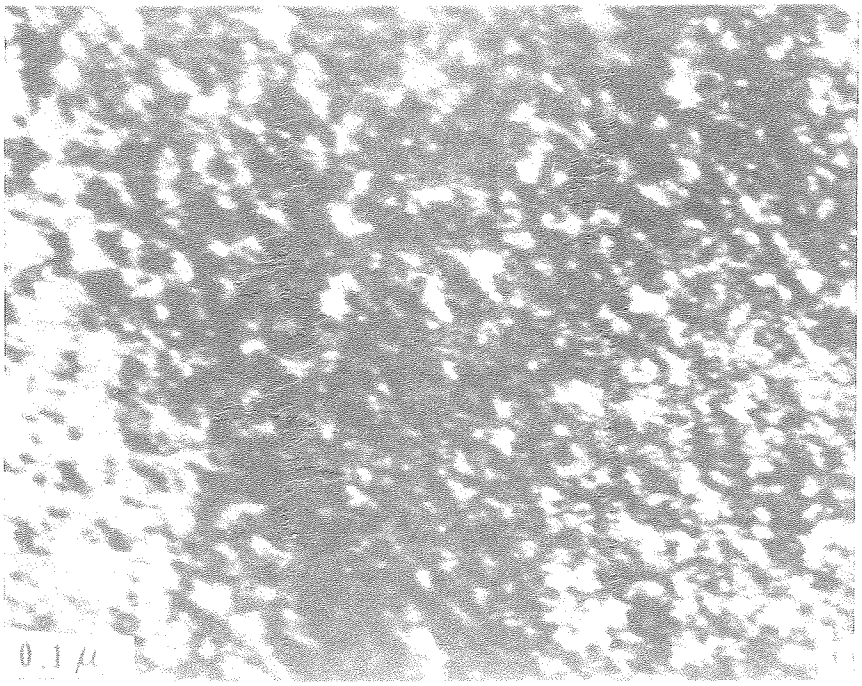

XBB760-10139

Fig. 12

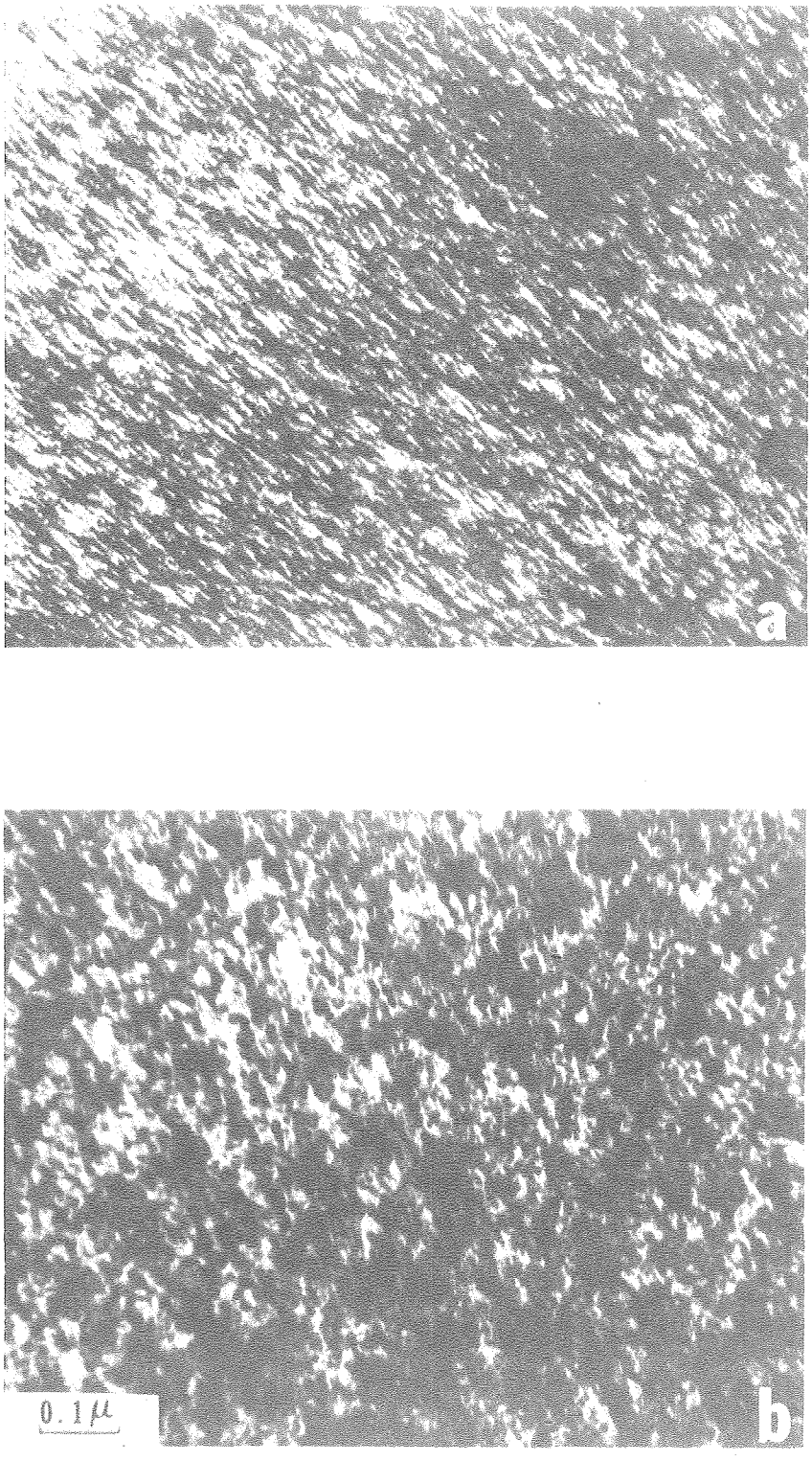

XBB760-10135

Fig. 13

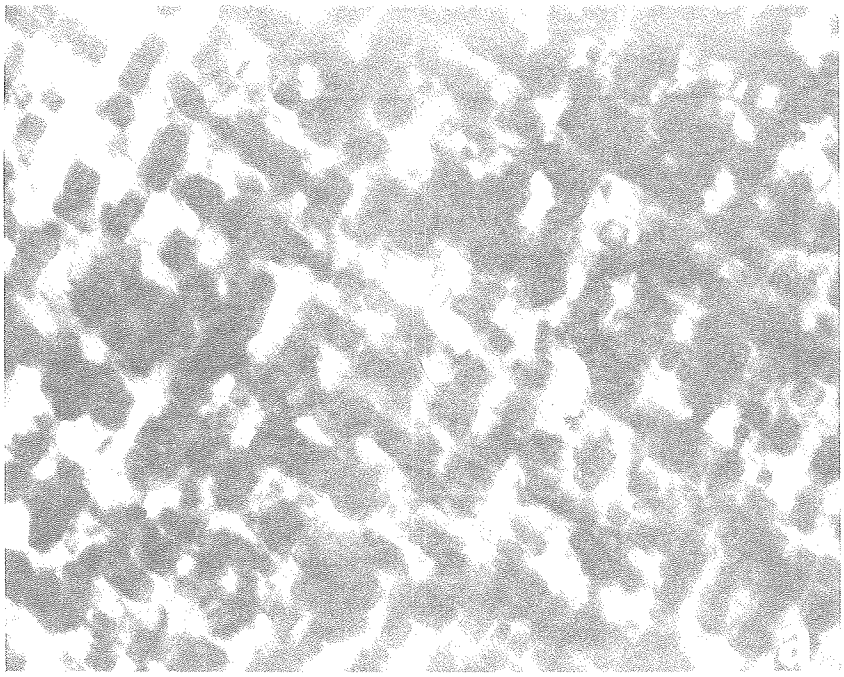

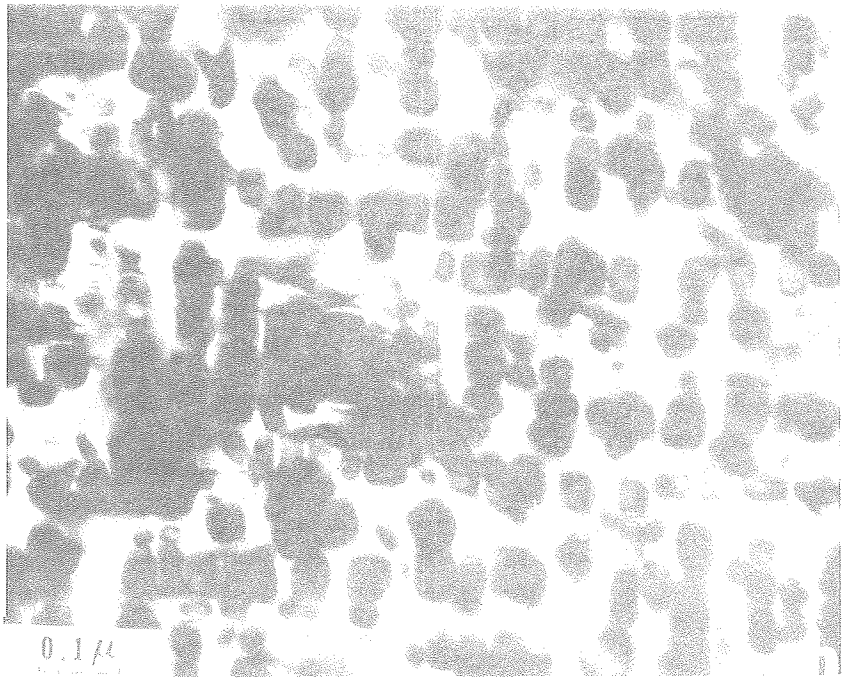

Fig. 14

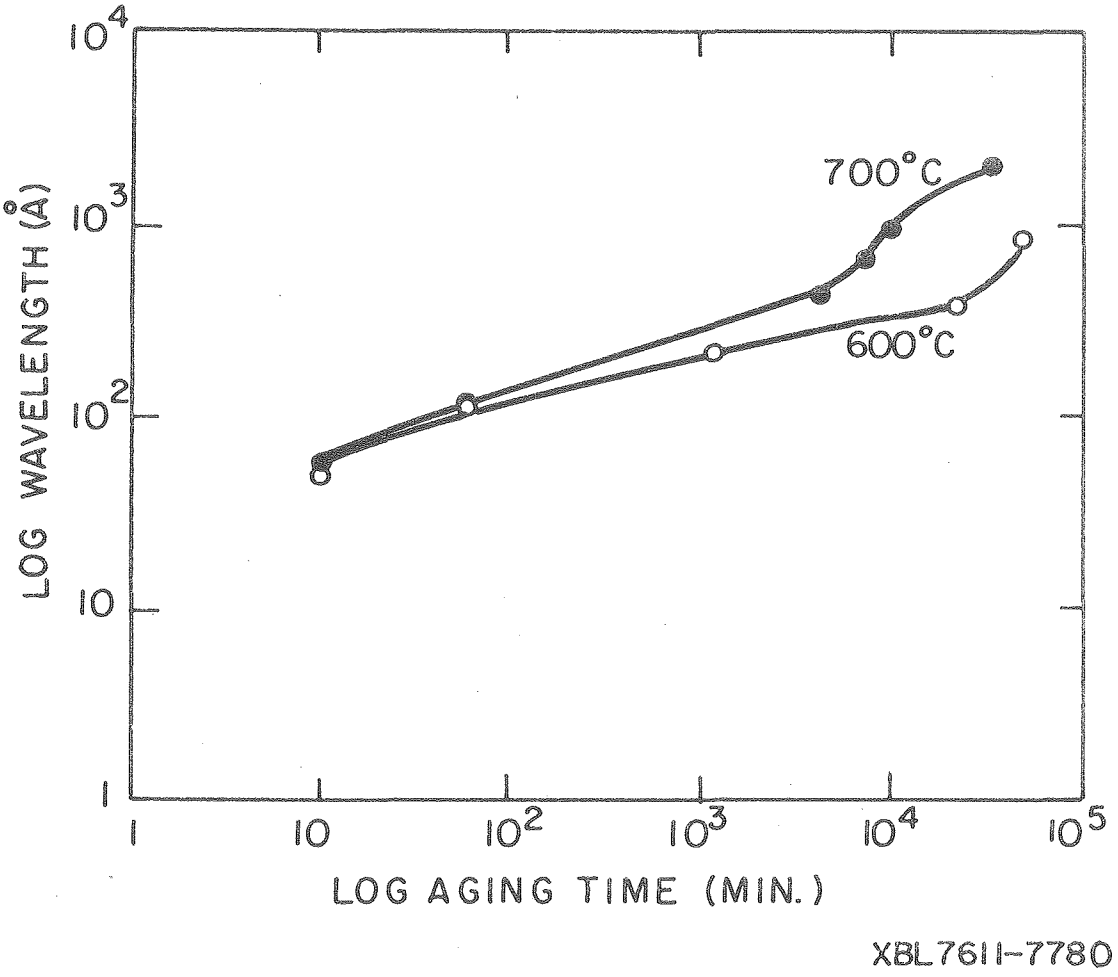
LOG WAVELENGTH (Å)
10^4
10^3
10^2
10
1
700°C
600°C
1
10
10^2
10^3
10^4
10^5
LOG AGING TIME (MIN.)
XBL7611-7780

Fig. 15

0 0 0 0 4 6 0 3 1 9 2

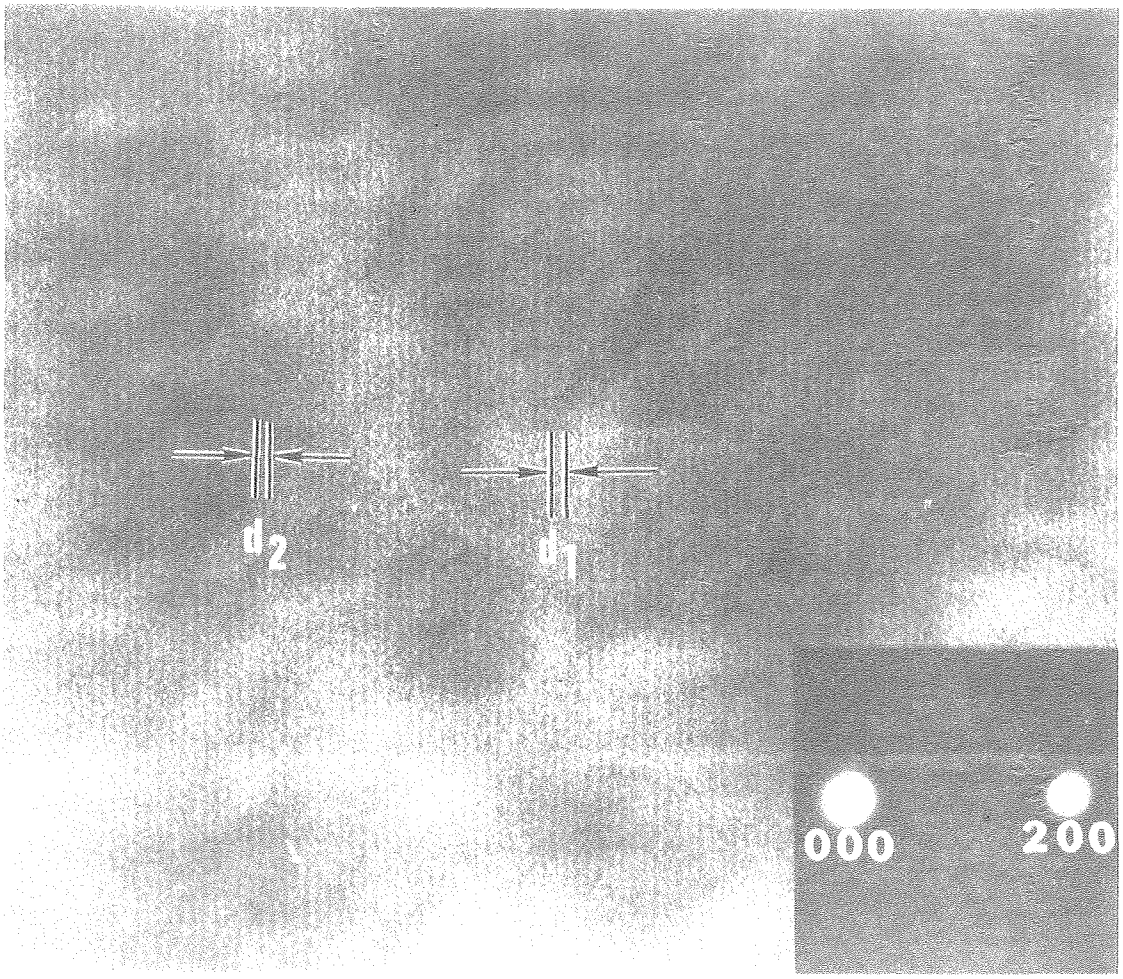

XBB 760-10136

Fig. 16

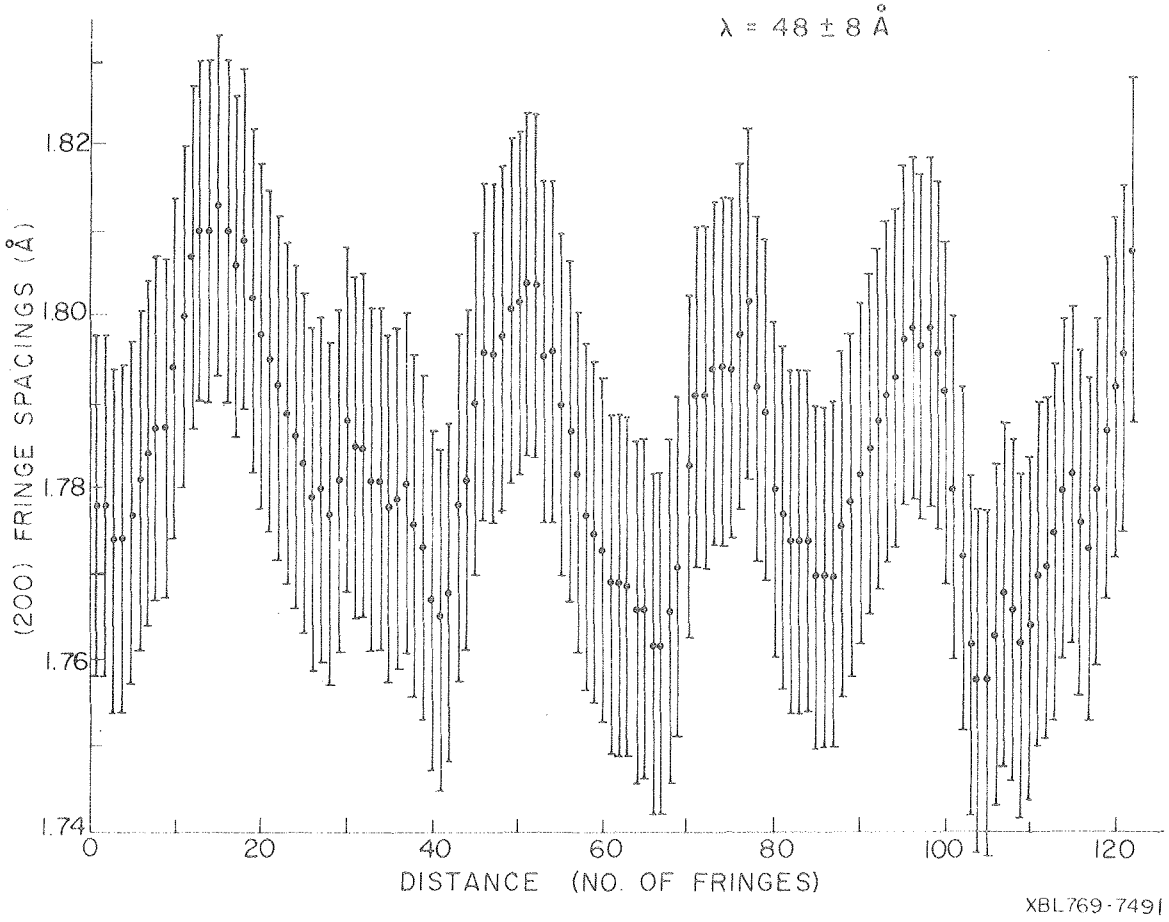
λ = 48 ± 8 Å
(200) FRINGE SPACINGS (Å)
1.82
1.80
1.78
1.76
1.74
0
20
40
60
80
100
120
DISTANCE (NO. OF FRINGES)
XBL769-7491

Fig. 17

0 0 0 0 4 6 3 8 1 9 3

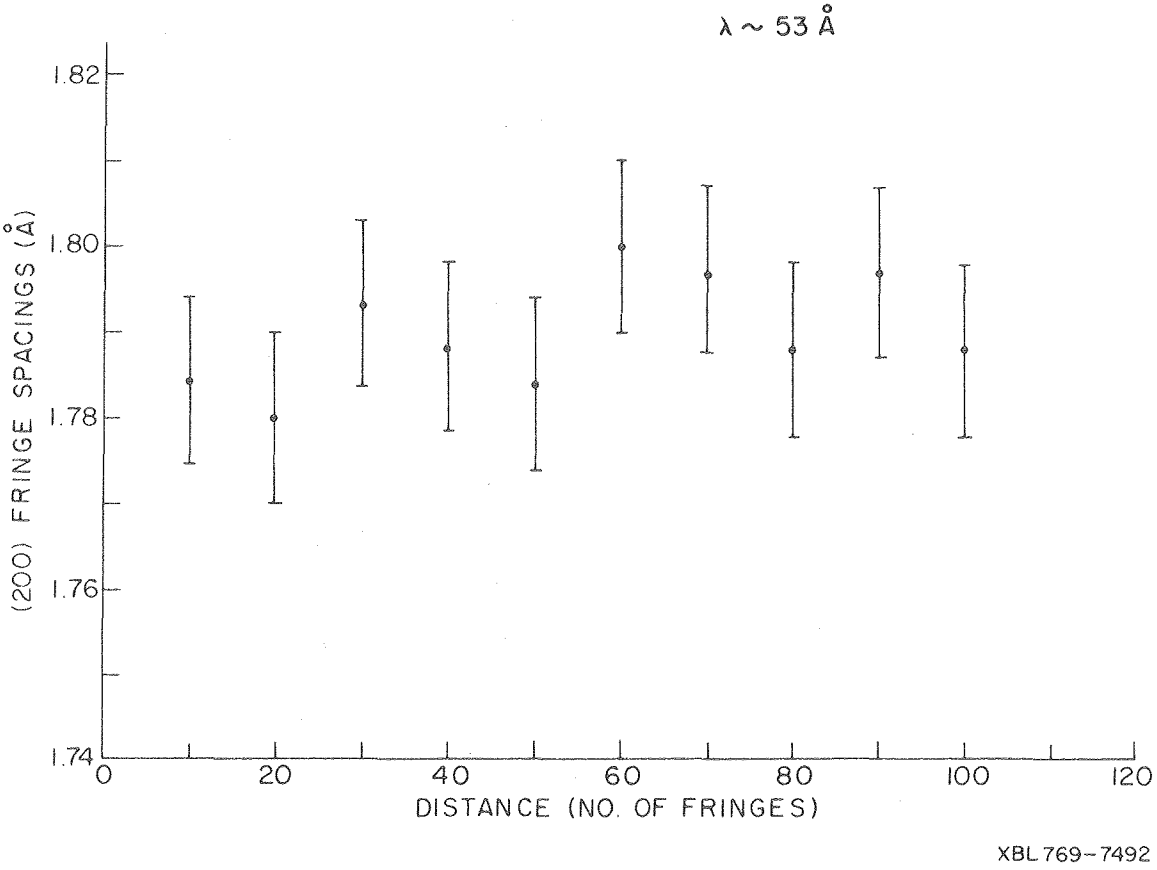

Fig. 18

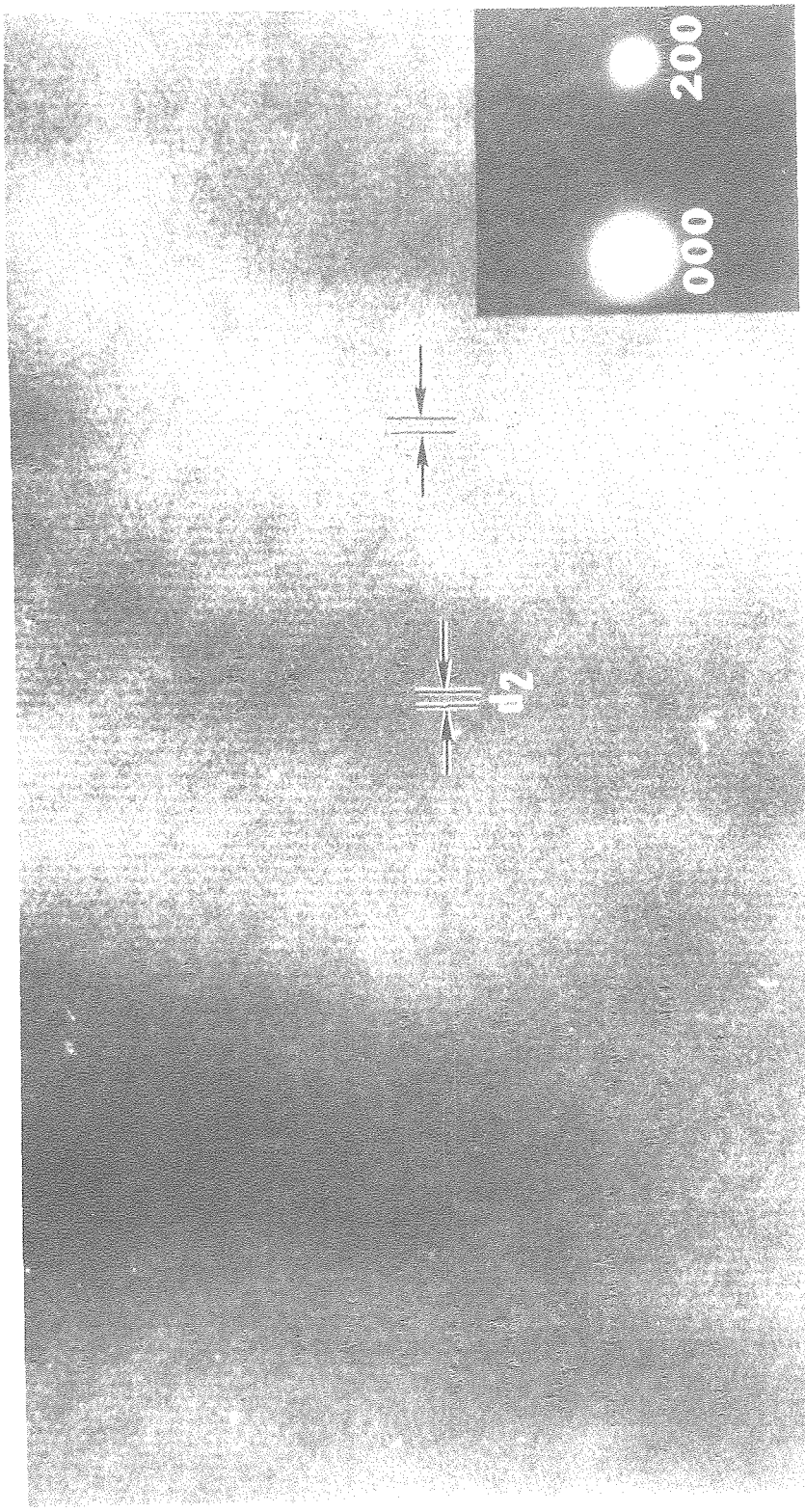

XBB760-10137

Fig. 19

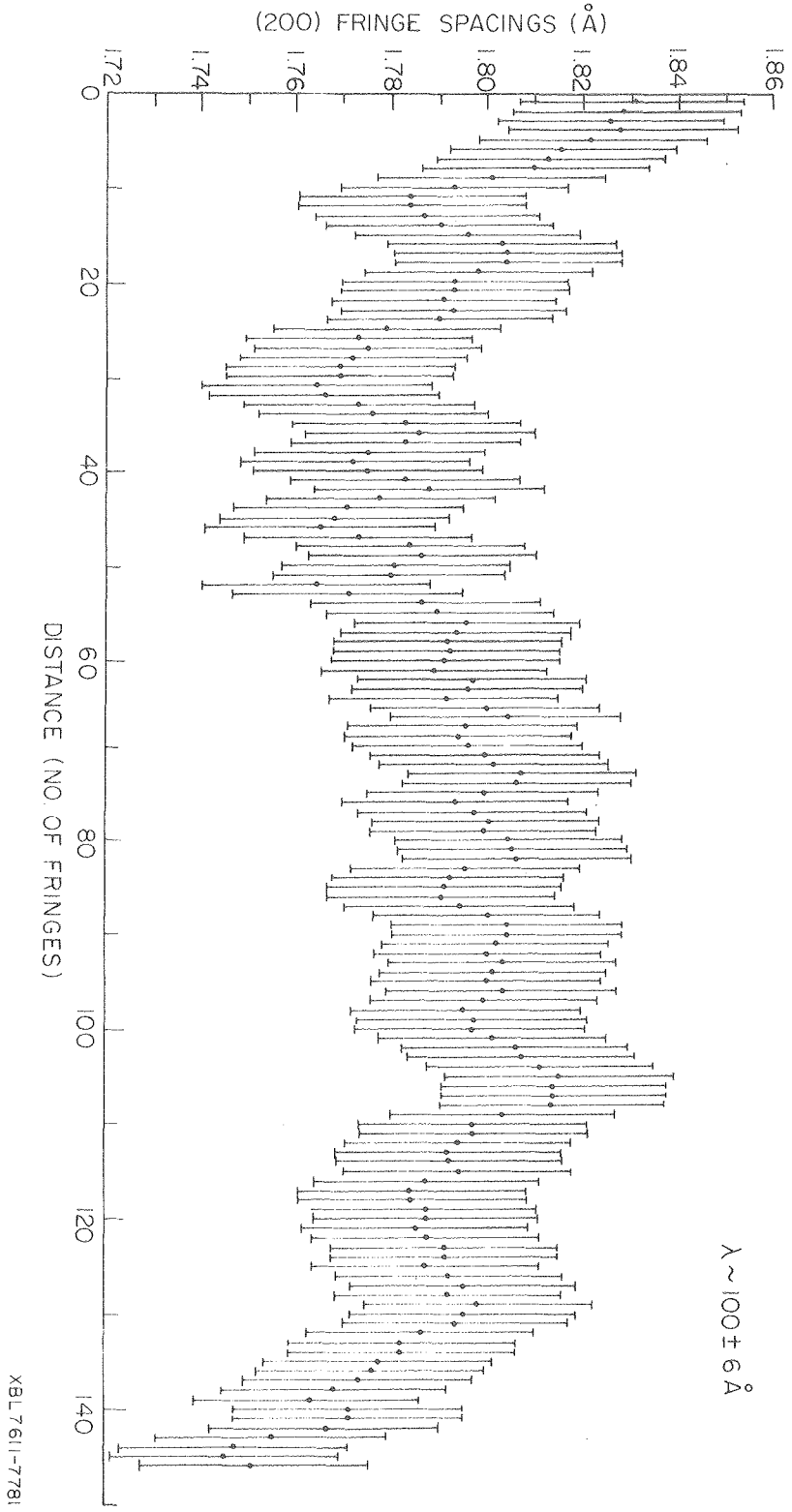
(200) FRINGE SPACINGS (Å)
1.72
1.74
1.76
1.78
1.80
1.82
1.84
1.86
0
20
40
60
80
100
120
140
DISTANCE (NO. OF FRINGES)
λ ~ 100 ± 6 Å
XBL 7611-7781

Fig. 20

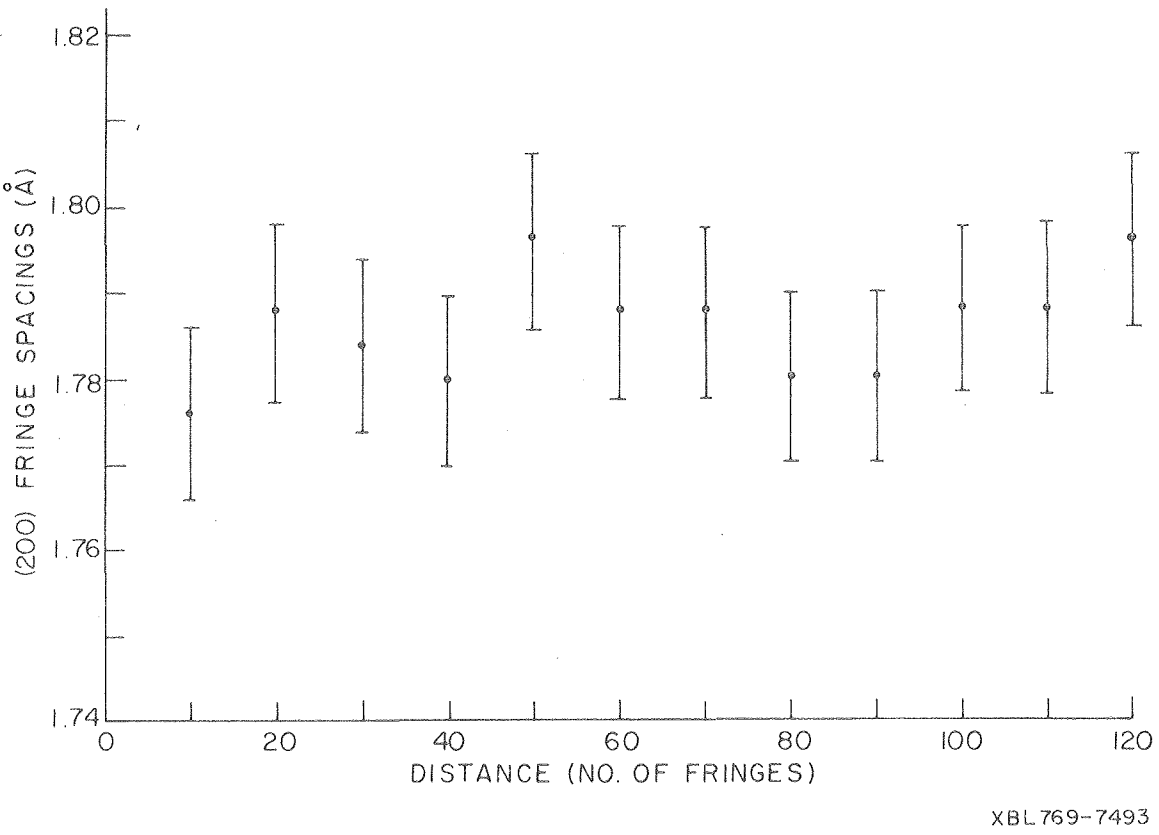
1.82
1.80
1.78
1.76
1.74
(200) FRINGE SPACINGS (Å)
0
20
40
60
80
100
120
DISTANCE (NO. OF FRINGES)
XBL769-7493

Fig. 21

0 0 0 0 4 6 0 8 1 9 4

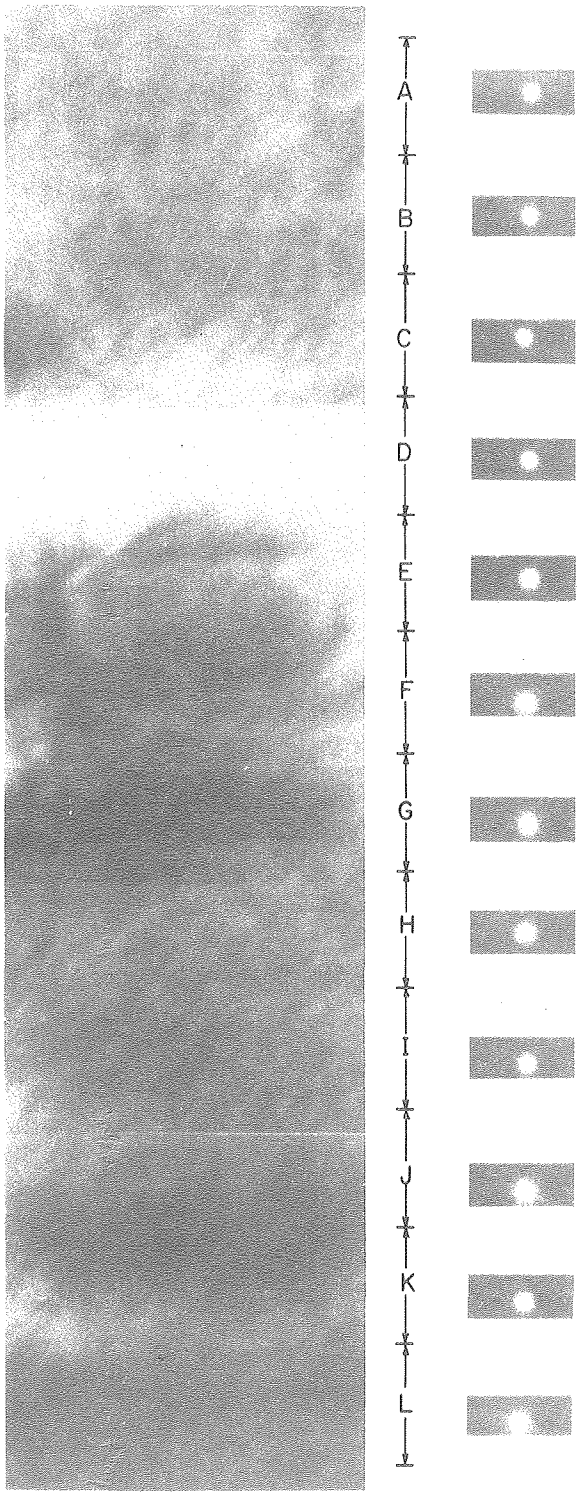

Fig. 22

XBB 769-7992

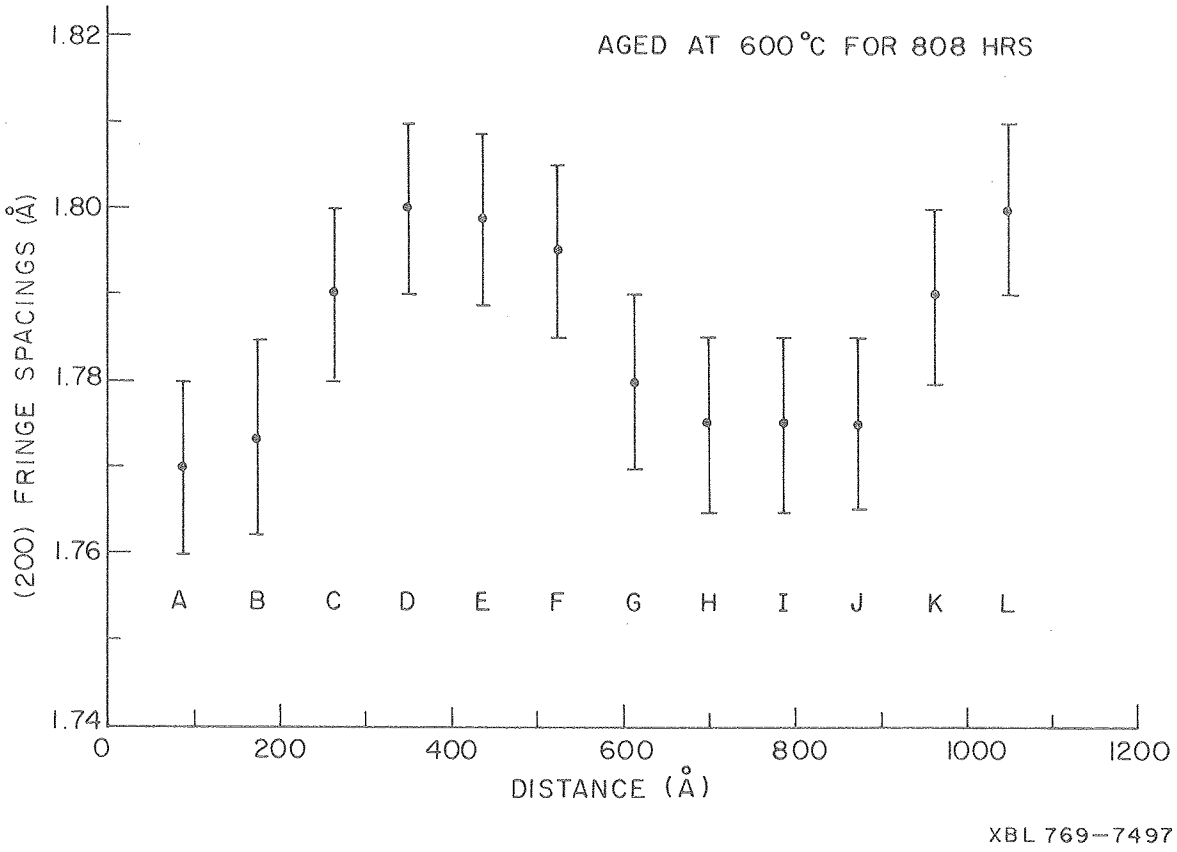
AGED AT 600°C FOR 808 HRS
(200) FRINGE SPACINGS (Å)
1.82
1.80
1.78
1.76
1.74
A
B
C
D
E
F
G
H
I
J
K
L
0
200
400
600
800
1000
1200
DISTANCE (Å)
XBL 769-7497

Fig. 23

0 0 0 0 4 6 0 3 1 9 5

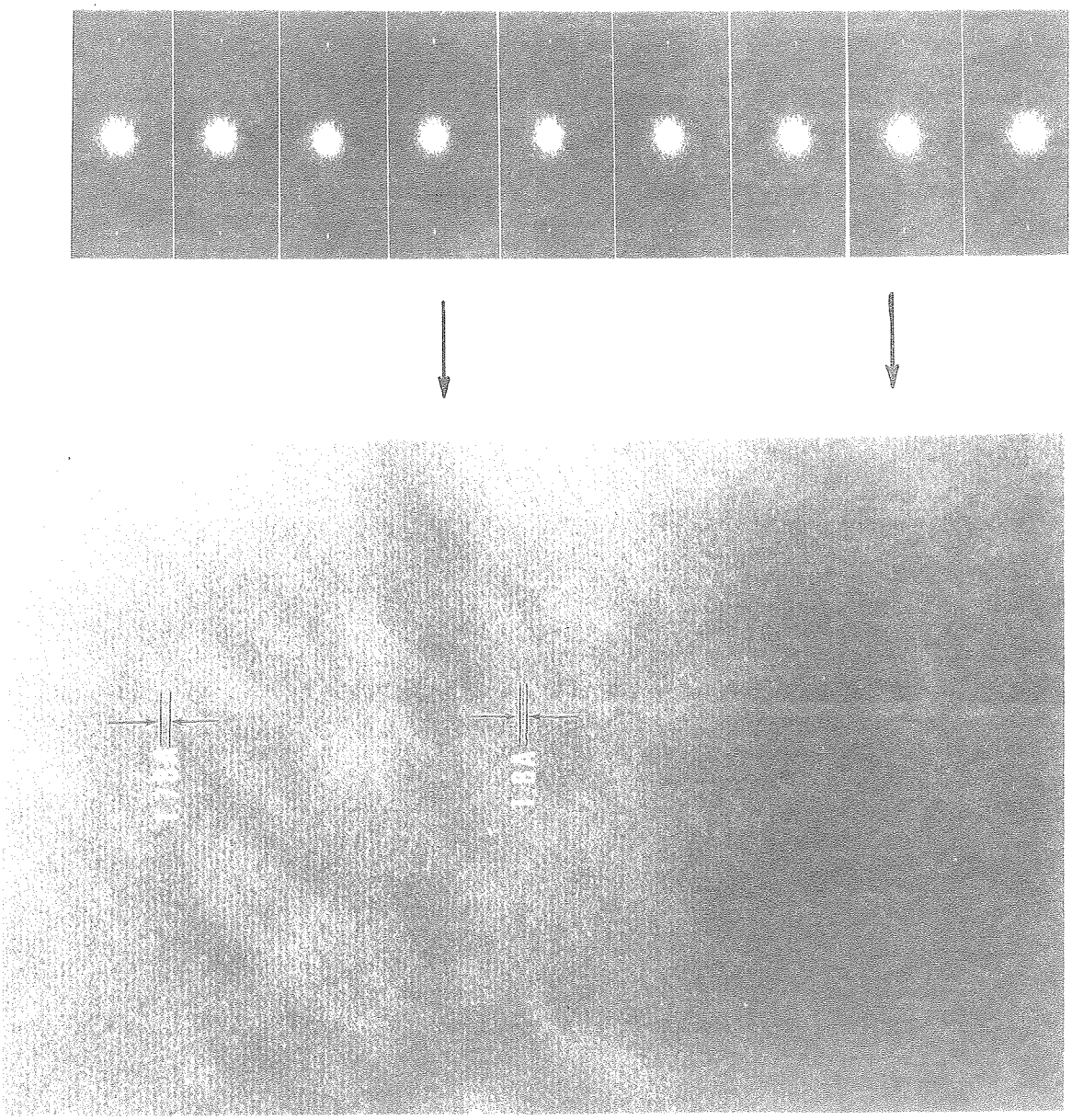

XBB760-10126

Fig. 24

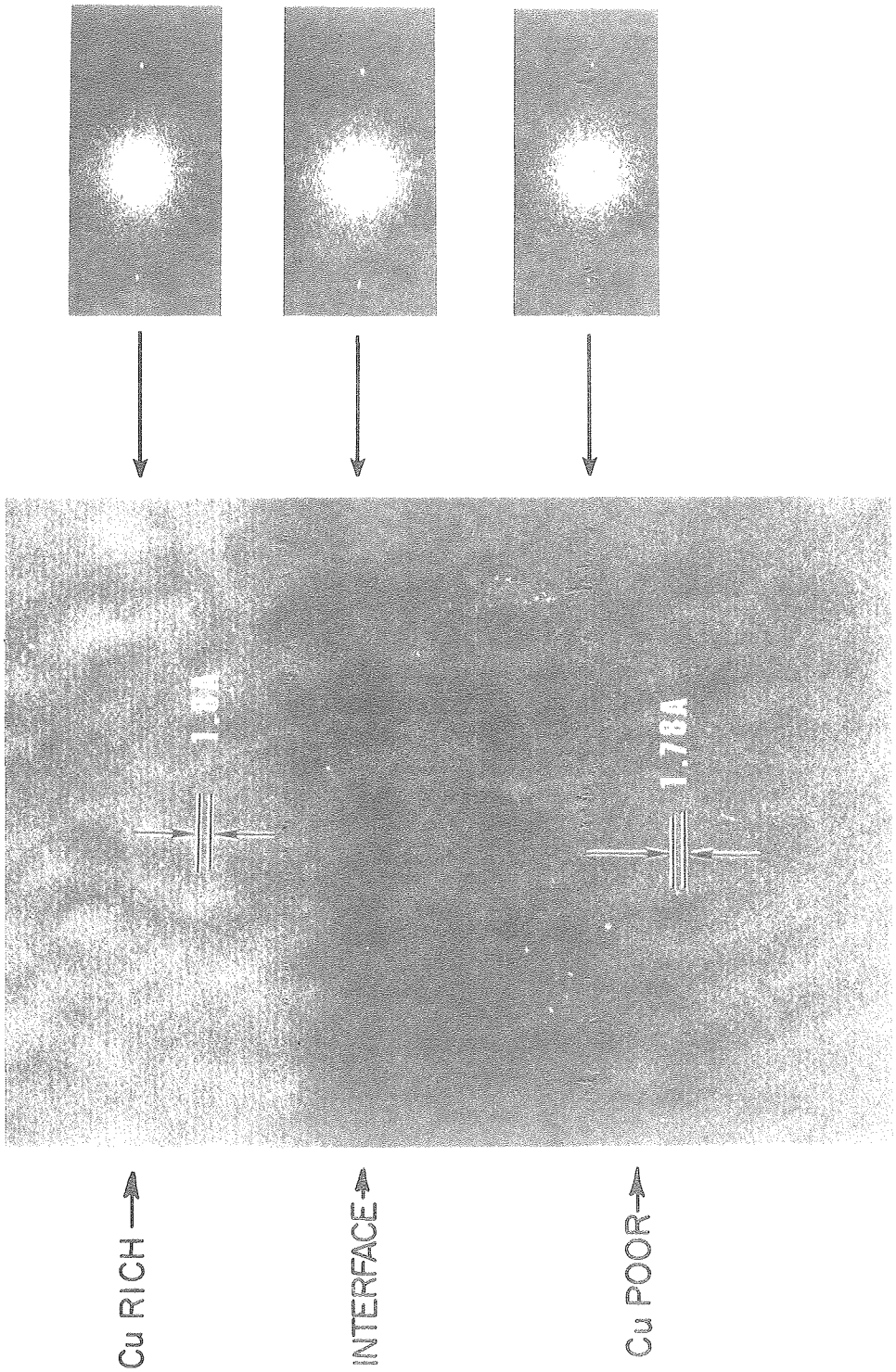

XBB760-10131

Fig. 25

0 0 0 0 4 6 0 3 1 9 6

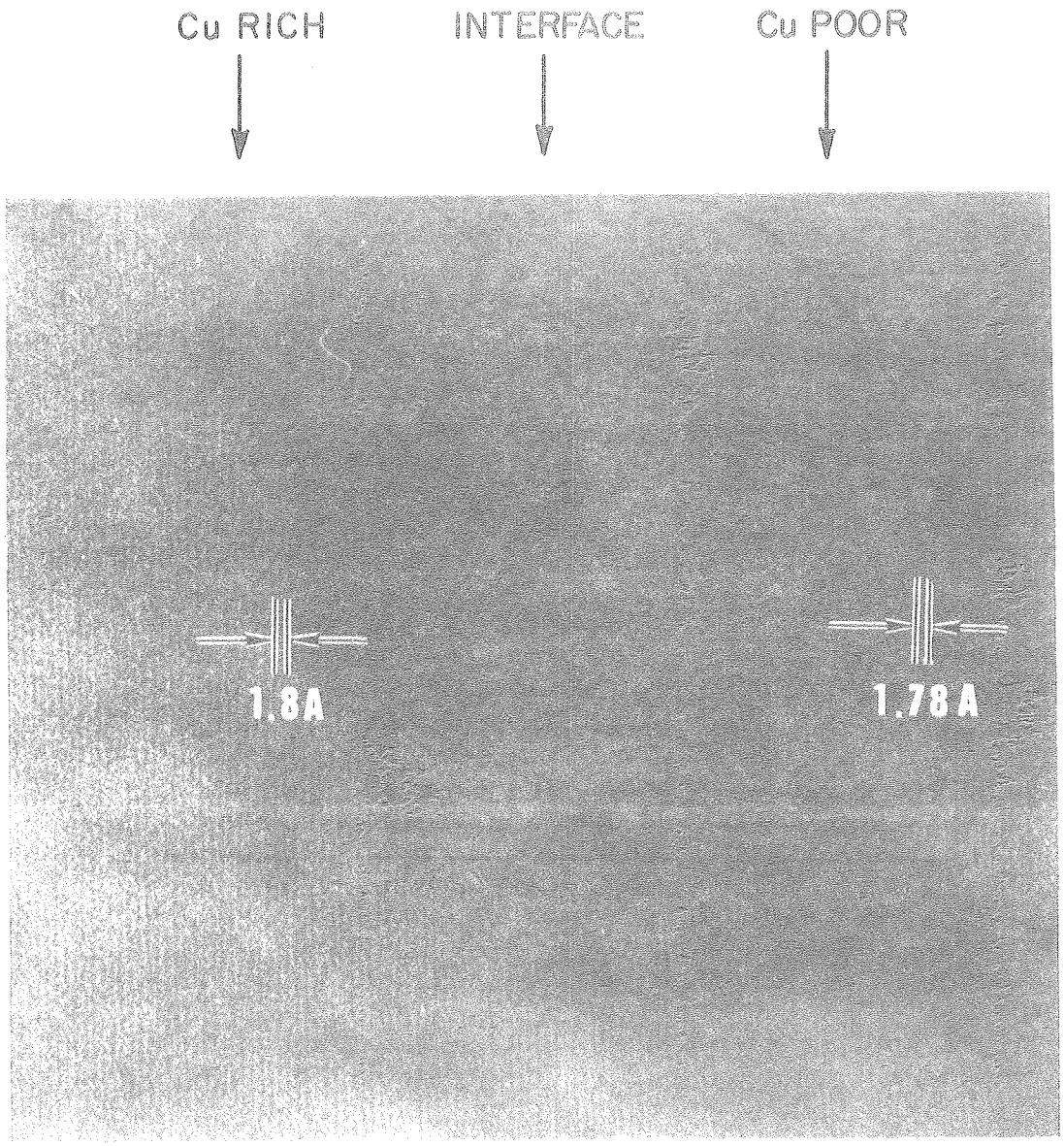

XBB760-10141

Fig. 26

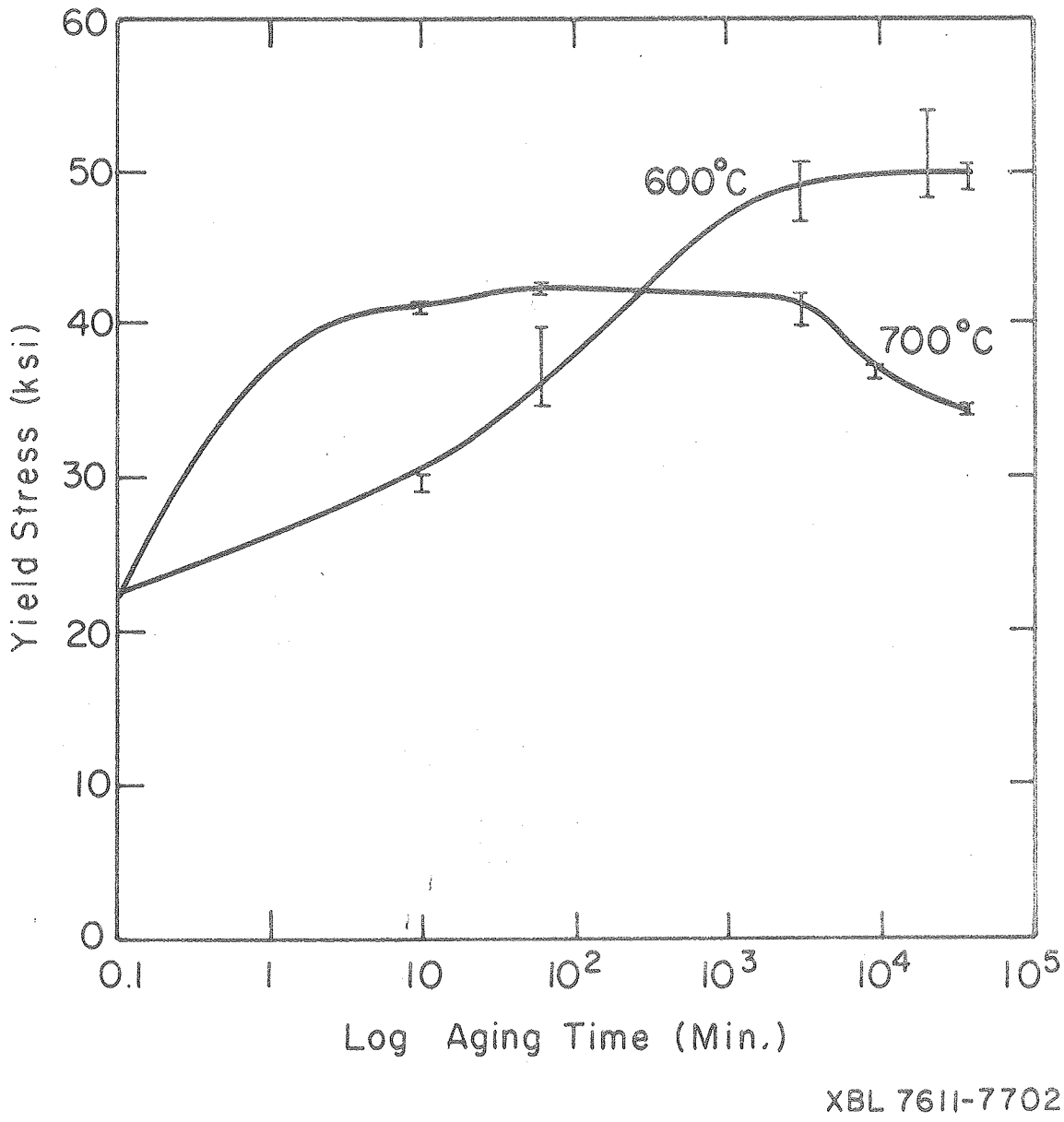
60
50
40
30
20
10
0
Yield Stress (ksi)
600°C
700°C
0.1
1
10
10²
10³
10⁴
10⁵
Log Aging Time (Min.)
XBL 7611-7702

Fig. 27

0 0 0 0 4 6 0 8 1 y 7

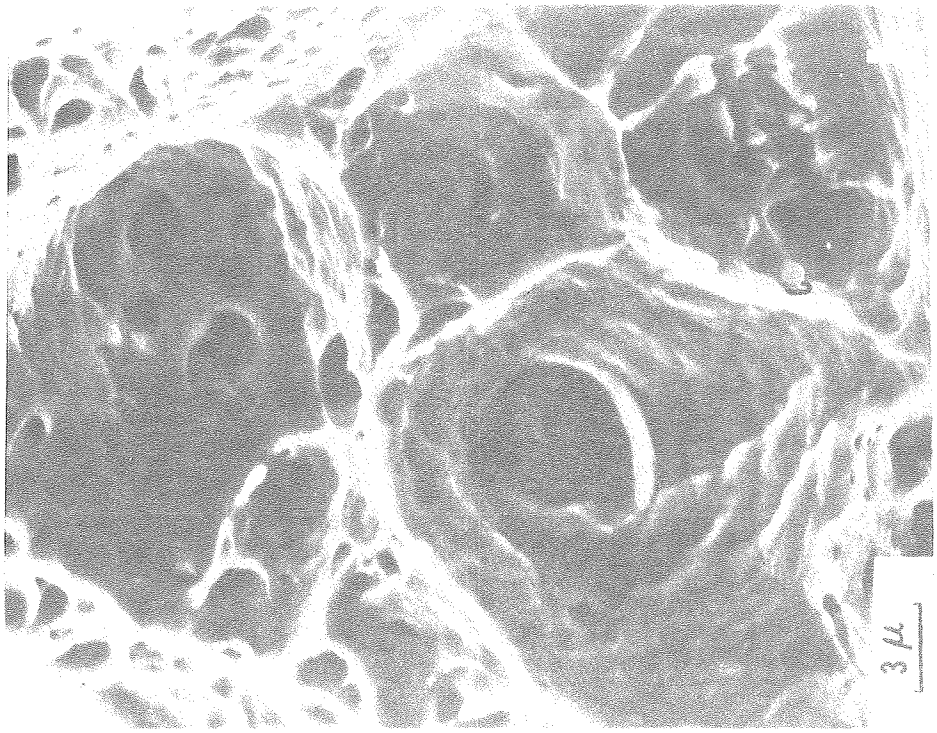

XBB760-10129

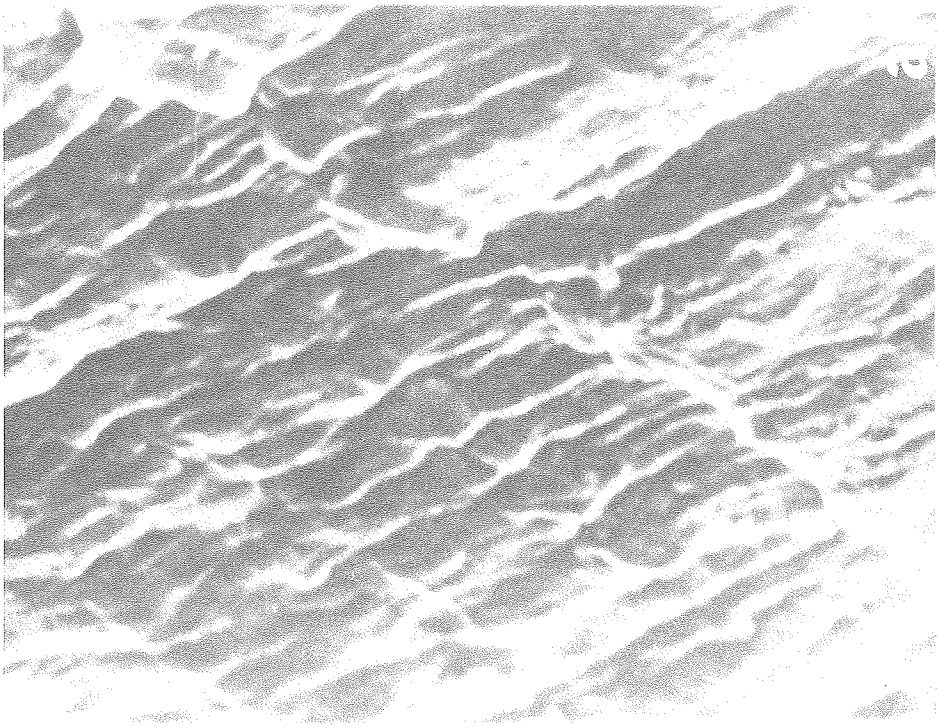

Fig. 28

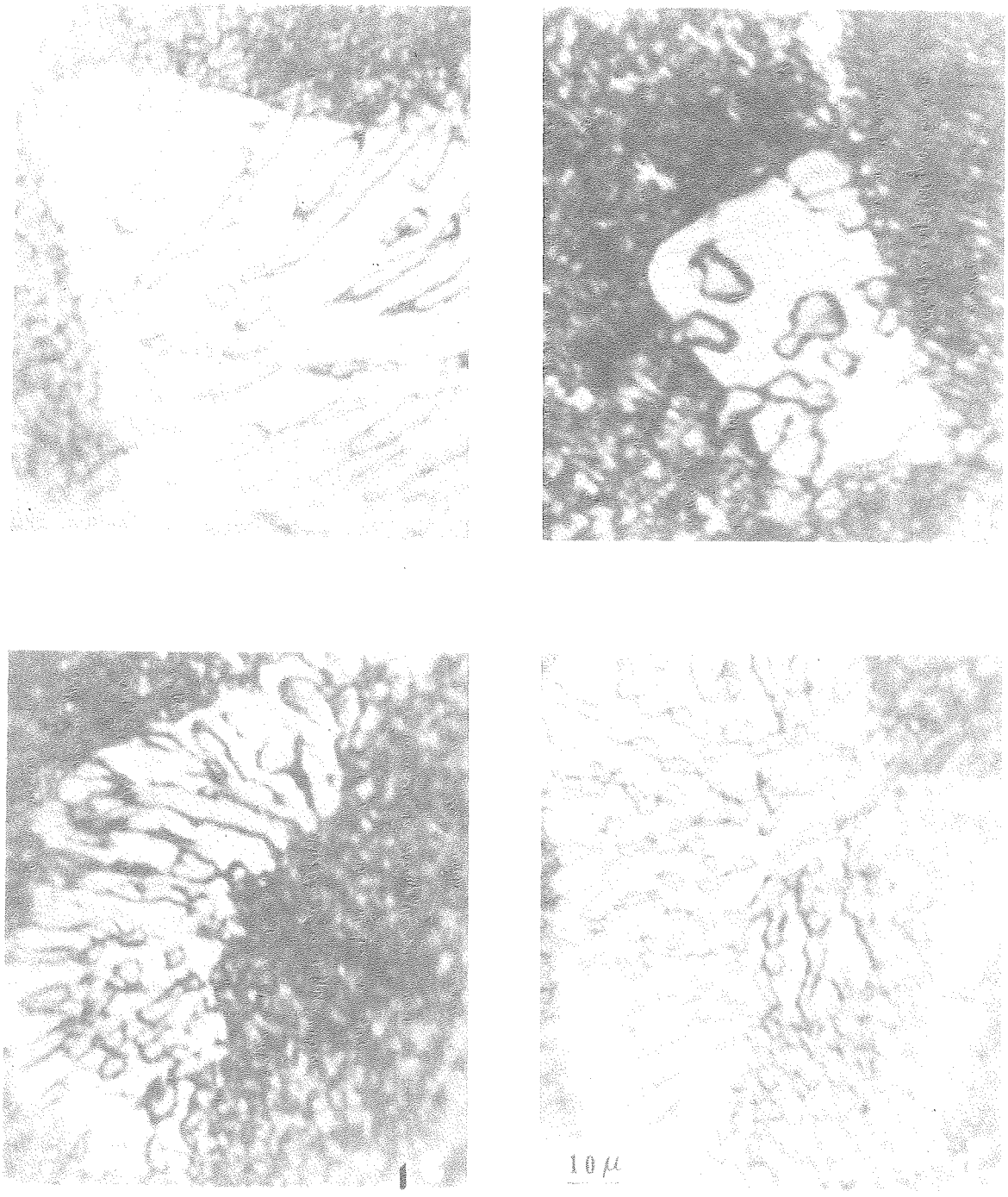

XBB760-10130

Fig. 29

0 0 0 0 4 6 3 3 1 9 8

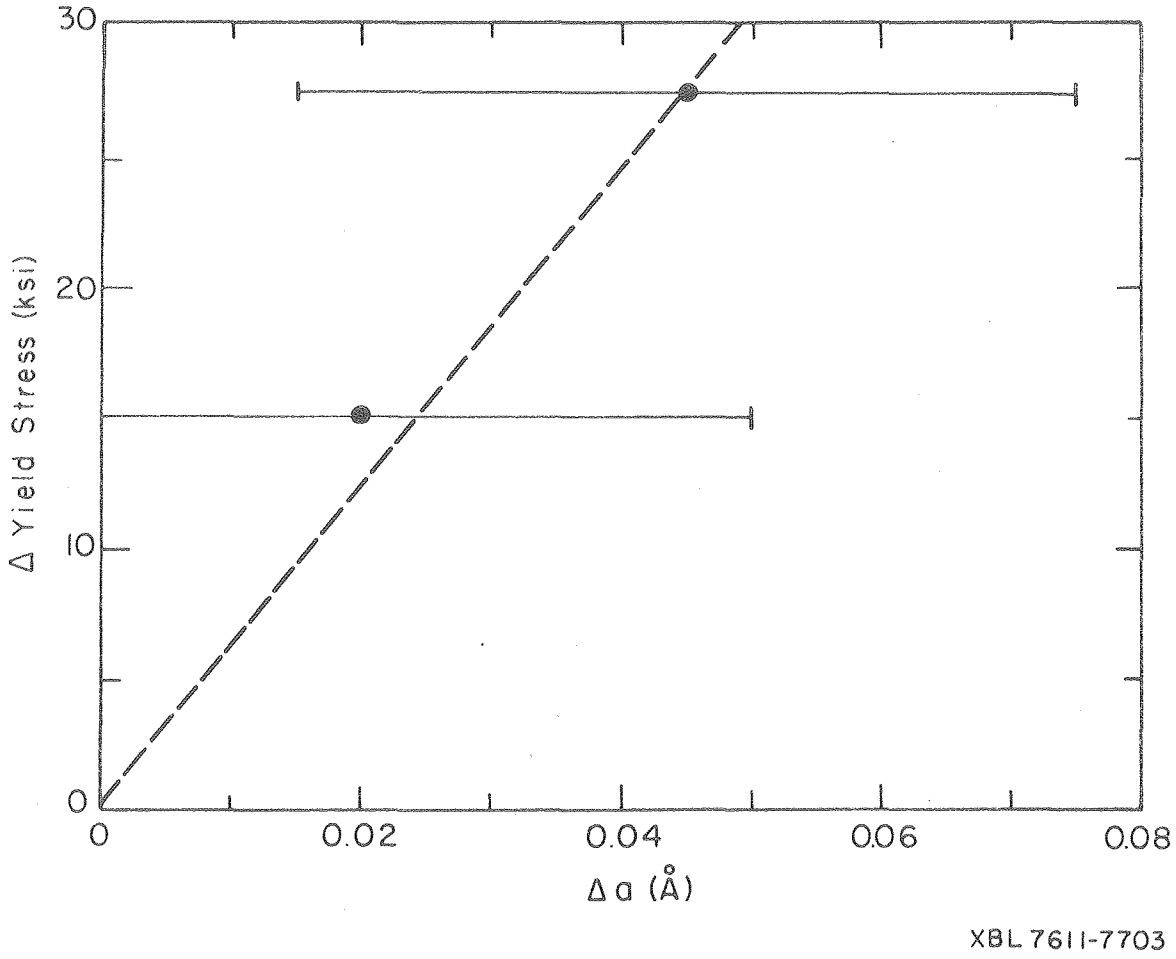

Fig. 30

This report was done with support from the United States Energy Research and Development Administration. Any conclusions or opinions expressed in this report represent solely those of the author(s) and not necessarily those of The Regents of the University of California, the Lawrence Berkeley Laboratory or the United States Energy Research and Development Administration.

0 0 0 0 4 5 0 2 2 9 4